

Maria Teige

Experimental investigation of drag and lift forces on hydroid fouled nets

Master's thesis in Marine Technology
Supervisor: Pål Furset Lader
June 2019

Maria Teige

Experimental investigation of drag and lift forces on hydroid fouled nets

Master's thesis in Marine Technology
Supervisor: Pål Furset Lader
June 2019

Norwegian University of Science and Technology
Faculty of Engineering
Department of Marine Technology

Summary

Marine biofouling is growing on nylon nets used for fish farming and it is a serious problem for the industry. It affects fish health and welfare and gives larger loads to the net pen itself. The hydroid *Eruetra Larnyx* is the most abundant type of biofouling in Norwegian waters. Some of the reasons are that hydroids are very versatile, have a quick life cycle and are reproduced easily. Elimination of the hydroids by high-pressure *in situ* cleaning does not completely remove them, seeing that regenerative parts may remain. Fouling of hydroids on nets will therefore always remain an issue for fish farmers.

The calculation of forces on a fish pen is regulated by the national standard NS9415. Forces on a fouled net are accounted for by increasing the twine diameter of the net by 50%. This thesis researches the forces acting on a bio fouled net section with different solidities and angles of attack. The aim is to find connections of the variables and estimate a functional relationship of drag and lift coefficients on a net. This will give perhaps give justification to the method in use or produce a more reliable coefficient for estimating loads on a bio fouled net.

Experimental investigation of the forces is done by towing tests in the Marine Cybernetics laboratory at NTNU facilities in Trondheim. Clean and fouled twine models are made from two 1.5 mm steel rods twisted together. The artificial hydroids made of 0.32 mm multifilament fishing line is fixed in between. It replicates a 3 mm twine in the net with a hydroid length of 16 mm and a density of 1.4 hydroids/mm. The twines are configured as net panels with a solidity of 0.28, 0.237 and 0.19. They are tested for angles of attack of 0°, 10°, 20°, 30° and 45° and velocities of 0.05, 0.1, 0.2, 0.25, 0.3 and 0.35 m/s. It is of interest to look at low Reynolds number since similar experiments have not been done so far. The uncertainty of the measurements is based on repeated tests and calculated by student-t distribution.

Both drag and lift on nets with biofouling are amplified significantly due to the presence of hydroids. The dependency of the angle of attack and solidity is clear. Drag measurements are validated as coefficients of the clean net panel is similar to the estimation by Løland (1991). Lift on the other hand has too many negative values and large uncertainty which gives diverse results. The drag coefficients on fouled nets are defined as independent of Reynolds number for the tested range of 300 - 1100 *Re*. The dependency on both solidity and angle of attack is greater for fouled nets. It appears that the deformation of the hydroids on net panels is greater for larger angles of attack. In addition, the extra projected area from the hydroids is increasing with solidity, which escalates the drag forces with increasing solidity. Since the lift coefficient on clean nets does not follow the expected trend, it is unknown if the results are due to a bias error for lift measurements or a phenomenon of the hydroids.

An update to assure technical approval for fouled nets in NS9415, is a new formula for the drag coefficient based on the solidity and angle of attack.

Sammendrag

Marine begroing vokser på nett som brukes til oppdrett, og det er et alvorlig problem for bransjen. Det påvirker fiskens helse og velferd, og i tillegg fører den til større belastninger på notposen. Hydroiden *Eruetra Larnyxis* er den mest utbredte typen begroing i norske farvann. Noen grunner til dette er at hydroidene er allsidige, har en rask livssyklus og reproducerer seg fort. Eliminering av hydroider ved høytrykksspyling under vann er ikke komplett, da regenerative deler av hydroidene kan forbli. Begroing av hydroider på nett vil derfor alltid være et problem i næringen.

Beregning av kreftene på en installasjon for oppdrett, er regulert av nasjonal standard NS9415. Kreftene på et begrodd nett tas hensyn til ved å øke nettets tråddiameter med 50%. Denne masteroppgaven undersøker drag- og løftekreftene som virker på et begrodd nett, i forhold til nettets soliditet og strømmens angrepsvinkler. Målet er å finne koblinger mellom variablene, og anslå et funksjonelt forhold til drag- og løftekoeffisienter på et nett. Det vil muligens gi berettigelse til metoden som er i bruk, eller produsere en mer pålitelig koeffisient for å estimere belastninger på et begrodd net.

Eksperimentell forskning av kreftene gjøres ved slepetester i Marine Kybernetikk laboratoriet hos NTNU på Tyholt, Trondheim. Rene og begrodd trådmodeller er laget av to 1,5 mm stålstenger som er vridd sammen. De kunstige hydroidene er laget av 0,32 mm multifilament fiskesnøre er festet imellom. De replikerer en 3 mm tråd i nettet, med hydroid lengde på 16 mm og tetthet på 1,4 hydroider / mm. Modellene er konfigurert som nettpaneller med soliditet på 0,28, 0,237 og 0,19. Alle er testet for angrepsvinkler på 0°, 10°, 20°, 30° og 45° og for strømhastigheter på 0,05, 0,1, 0,2, 0,25, 0,3 og 0,35 m / s. Det er interessant å undersøke lave Reynolds tall siden ingen lignende eksperimenter har gjort det. Usikkerheten til målingene er basert på gjentatte tester og beregnet ved Student't-distribusjon.

Drag og løft på begrodd net forsterkes betraktelig på grunn av tilstedeværelsen av hybrider. Avhengigheten av angrepsvinkel og soliditet er tydelig. Målinger av drag er validert ettersom koeffisientene til det rene nettpanleet, ligner estimeringen av Løland (1991). Målingene av løft, har på den andre siden for mange negative verdier og stor usikkerhet, som gir ulike resultater. Dragkoeffisienter på begrodd net er definert som uavhengig av Reynolds-tall for det testede området på 300 - 1100 *Re*. Avhengigheten av både soliditet og angrepsvinkel er større for begrodd net. Det ser ut til at deformeringen av hydroider på nettpaneller blir mer omfattende for større angrepsvinkler. I tillegg øker det ekstra projiserte området fra hydroidene med soliditet, som igjen eskalerer dragkraften med økende soliditet. Siden løftekoeffisienten på rene net ikke følger den forventede trenden, er det ukjent om resultatene skyldes en biasfeil eller om det er et fenomen av hydroidene.

En oppdatering for å forsikre teknisk godkjenning av begrodd net i NS9415, er en ny formel for drag koeffisient basert på soliditeten og angrepsvinkelen.

Preface

This master thesis is written during the spring of 2019 as a part of my studies for a Masters of Science degree in Marine Technology at The Norwegian University of Science and Technology (NTNU) in Trondheim. It is the final assessment of the course TMR4930. The master thesis is written over a period of 20 weeks. The candidate number for this master thesis is 10019.

I am very grateful to my supervisor, Professor Pål Furset Lader, for guidance and advise throughout the semester. Thank you for the opportunity to complete such a fun experimental thesis and for giving me confidence in my abilities. I would also like to thank lab engineer Trond Innset and mechanical technician Ole Erik Vinje at NTNU, for helping to build the models. Lab technician Thorgeir Walh has also been very helpful and assisted in calibration and set up in the tank. Thank you to Luca Savio for recommendations with the post-processing of results.

I would like to thank my fellow students, for valuable discussions and giving feedback in the writing process. Especially the people at my office, thank you for all the good laughs and many coffee breaks. Finally, I would like to thank my family and friends for their never ending support.



Trondheim, June 10, 2019
Maria Teige

Table of Contents

Summary	i
Sammendrag	ii
Preface	iii
Table of Contents	vi
List of Tables	vii
List of Figures	xi
Abbreviations	xii
1 Introduction	1
1.1 Background	1
1.2 Problem description	2
1.3 Scope and limitations	3
2 Literature Review	5
2.1 The net cage	5
2.2 Forces on a submerged cylinder	6
2.3 Modelling of loads on a submerged net	7
2.4 Fouling of net cages	8
2.5 Results from project thesis	11
2.6 Experimental testing	16
3 Method	19
3.1 Pre-experiment	19
3.1.1 Flow disturbances	19
3.1.2 Conceptual choices	20
3.1.3 Expectation of forces	22

3.2	Production of model	23
3.2.1	Frame	23
3.2.2	Clean and fouled twines	24
3.3	Assembly	29
3.3.1	Calibration and data acquisition	29
3.3.2	Setup	30
3.4	Experiments	32
3.5	Post processing	35
3.5.1	Analysis	35
3.5.2	Decay test	39
3.5.3	Forces on net section	40
3.6	Accuracy and precision	41
4	Results and Discussion	45
4.1	Mean drag and lift forces on net section	45
4.2	Drag and lift coefficients	48
4.3	Comparison to Lader	50
4.4	Comparison to Løland	51
4.4.1	Clean twines	51
4.4.2	Twines with biofouling	56
4.5	Errors	63
5	Conclusions	65
5.1	Experimental testing	65
5.2	Recommendations for further work	66
	Bibliography	69
	Appendix	71
5.3	Flow past a dipole	71
5.4	Production	72
5.5	List of Excel sheets and Matlab codes	73
5.6	Post processing	75
5.7	Uncertainty	77
5.8	Coefficients on clean twines	77
5.9	Comparison with Løland	79
5.10	Functions of trend lines	82

List of Tables

3.1	Parameters for the experiments	21
3.2	Constants used for the models	22
3.4	Drag data	42
3.5	Lift data	42
3.6	Uncertainty drag	43
3.7	Uncertainty lift	44
3.8	Uncertainty velocity	44
4.1	Percentage decrease of the drag forces with over angle 0° - 45°	59
5.1	Equipment used in the process of making the twines	72
5.2	Carriage speed data	77

List of Figures

2.1	Rachel knot less knitting. (Klebert et al., 2012)	5
2.2	A net consisting of physical twines with a length l_w and diameter d_w .	6
2.3	Drag and lift force on a submerged cylinder (twine).	7
2.4	The hydroid <i>Ectopleura larynx</i> fouling a salmon net in Norway during late summer. Photograph by Leif Magne Sunde – SINTEF. Taken from De Nys and Guenther (2009).	9
2.5	Main parts of <i>Ectopleura larynx</i> . The illustration is inspired by Hayward and Ryland (1990).	10
2.6	Overview of the three stages of <i>E. larynx</i> to maintain their settlement to the net. Taken from (Guenther et al., 2011)	11
2.7	Curve fits and data points showing drag coefficient for Reynolds number and the estimation from Hoerner. Taken from Lader et al. (2015).	12
2.8	Relationship between growth period, hydroid length and drag coefficients for different Reynolds numbers. Taken from Lader et al. (2015).	12
2.9	Percentage difference to Morrison type increased drag force	13
2.10	Percentage difference to screen type increased drag force	13
2.11	Intersection of drag forces for a constant current velocity 0.346 m/s	14
2.12	Intersection of drag forces for a constant current velocity 1.04 m/s	15
2.13	Preliminary set up for experimental testing	17
3.1	Different flow regimes past a circular cylinder. Illustrations are inspired by Sunden (2011)	20
3.2	Illustration of the distance d , seen from above.	20
3.3	Two dimensional illustration of decomposed forces on a vertical twine with arbitrary orientation in a Morrison type force model. $F_N = \frac{1}{2} \rho C_D A (U \cos\theta)^2$	23
3.4	The towing wagon(green), back frame(blue), front frame(orange), rotating device (pink) and twines	24
3.5	Creating the artificial fouling	26
3.6	Drilling of twines	26

3.7	Models of twines with artificial fouling	27
3.8	Clamp fastening frame	28
3.9	Calibration of frame in lab	29
3.10	Setup	31
3.11	Cut interval in frame timeseries	37
3.12	Window error when $c = 3.0325$, $a = 2.7115/\sqrt{2}$, $f = 0.98$, $ts = 15$	37
3.13	Window error when $c = 0.1945$, $a = 1.2135/\sqrt{2}$, $f = 6.281$, $ts = 33$	38
3.14	Test done on the last day at 0°	39
3.15	Test done at 30°	40
3.16	Net section	41
4.1	Mean drag and lift on fouled and clean section of 16 twines	46
4.2	Mean drag and lift on fouled and clean net section of 14 twines	47
4.3	Mean drag and lift on fouled and clean net section of 12 twines	47
4.4	Drag and lift coefficients on fouled net sections	49
4.5	Experimental data of net section and curve fit of single twine from Lader et al. (2015)	50
4.6	Drag coefficient at 10° on clean nets	52
4.7	Drag coefficient at 45° on clean nets	52
4.8	Second degree polynomial trend line fitting drag measurements on clean net, plotted versus angle of attack, and Løland's estimation	53
4.9	Linear trend line fitting drag measurements on clean net, plotted versus solidity and Løland's estimation	53
4.10	Lift coefficient at 10° , on clean nets	54
4.11	Lift coefficient at 45° , on clean nets	55
4.12	Second degree polynomial trend line fitting drag measurements on clean net, plotted versus angle of attack, and Løland's estimation	55
4.13	Linear trend line fitting lift measurements on clean net, plotted versus solidity and Løland's estimation	56
4.14	Drag coefficients at 10° , on fouled nets	57
4.15	Drag coefficients at 45° , on fouled nets	57
4.16	Second degree polynomial trend line fitting drag measurements on fouled net, plotted versus angle of attack	59
4.17	Linear trend line fitting drag coefficients on fouled net, plotted versus over solidity	59
4.18	Lift coefficients at 10° , on fouled nets	60
4.19	Lift coefficients at 45° , on fouled nets	61
4.20	Second degree polynomial trend line fitting lift coefficients on fouled net, plotted versus angle of attack	62
4.21	Second degree polynomial trend line fitting lift coefficients on fouled net, plotted versus solidity. The clean net estimation follows a linear trend line	62
5.1	Wake past dipole	71
5.2	Thirsdays at 0°	75
5.3	Friday at zero°	76
5.4	Friday at 45°	76

5.5	16 twines, $S_n = 0.2820$	77
5.6	14 twines, $S_n = 0.2359$	78
5.7	12 twines, $S_n = 0.1989$	78

Abbreviations

d_w	=	twine diameter
l_w	=	twine length
m	=	half-mesh
U	=	current velocity
U_∞	=	ambient current velocity
Re	=	Reynolds number
ν	=	kinematic viscosity
ρ	=	Water density
A	=	Projected area of panel
Sn	=	Solidity
F_D	=	Drag force
F_L	=	Lift force
F_N	=	Normal force
θ	=	Angle of attack
C_D	=	Drag coefficient
C_L	=	Lift coefficient

Introduction

1.1 Background

Along the Norwegian coast, there are 986 locations producing farmed salmon. The young smolt is transported by well boats into floating fish cages at sea and farmed for about nine months until they reach a weight of 4.5 -5.0 kg. In every recent year, more than 1 400 000 tons of salmon have been produced. (Norwegian Directorate of Fisheries, 2017) The demand for the Norwegian quality salmon is globally large and it is exported at high rates.

Before the introduction of the Norwegian Standard NS9415 in 2003, little or no attention was paid to the technical challenges regarding expected forces at sea, risks of fish escape and fish welfare. The standard describes requirements for site surveys, risk analyses, design, dimensioning, production installation and operation. It includes a detailed description of the important forces to evaluate, as that is a crucial factor to reduce fish escape and genetic pollution. Current forces are one of the expected sea loads on fish pens. It is not a simple task to calculate current forces accurately, as the net cages are non-solid and flexible. The flow will partly go through and around the net cages. The hydrodynamic forces acting on the structure will affect its shape and the altered shape affects the hydrodynamic forces. Understanding the interaction of load and shape is complex for hydroelastic structures and has been researched by Lader and Enerhaug (2005), Lader et al. (2008) and Moe-Føre et al. (2016).

Marine biofouling growing on the twines of the net, is an addition to the complex calculation of current forces, among other negative impacts. Biofouling, or simply fouling, is a serious problem for the aquaculture industry. The problem affects fish health and welfare and gives larger loads to the net pen itself. The colonial hydroid *Ectopleura Larnyx* is the most common fouling organism on submerged nets in Norway. (Guenther et al., 2010) The nets serve as a safe habitat for hydroids to settle. They are versatile as they can and will attach to anything, have a quick lifecycle and are reproduced easily. Fouling has a very negative impact on the fish farm environment. It will decrease the performance of cleaner fish, infect gill health, threaten the internal volume of the net and alter the flow around the farm; resulting in a lower level of oxygen exchange. Elimination of hydroids by

high-pressure *in situ* cleaning does not completely remove the hydroid since regenerative parts may remain. The underwater pressure causes actinula to be released and it settles on the available cleaned net. (Carl et al., 2011) Fouling of hydroids on nets will therefore always be an issue for fish farmers.

It is desirable to understand both the biological effects and the technical aspects of fouling in aquaculture, to ensure a good design of the farm. Fouling is not included as a major concern in the design process of fish farms based on NS9415. However, fouling is accounted for by requiring to include a volume of fouling corresponding to 50% increase in the twine diameter. The increase in twine diameter is often referred to as the *fouling factor*. With this initiative, the calculated drag force on nets will be increased. The value of the twine increase has been accepted, but it is not studied in published research.

1.2 Problem description

The preliminary project thesis leading up to this master thesis investigated the fouling factor, set by national standards, in dimensioning drag loads on a fish farm. During this work, the experimental study done by Lader et al. (2015), was very important. In the study, it was researched how drag forces on single twines, parallel, single cross, and double cross developed with increasing current. All tests were done on with constant diameter of the twine and different lengths and densities of artificial hydroid fouling. The study presented drag coefficients in relation to Reynolds number for different lengths of artificial hydroid fouling and the relationship among growth period, hydroid length, and drag coefficient for different Reynolds numbers. A master thesis continued this work, expanding the experiments to include several twine configurations, using the same type of model. The configurations included different spacing between parallel twines and a closer representation of a net by adding eight twines in a net section. The relationship between the inflow angle, and the drag- and lift-forces for a fouled net has not yet been investigated.

The purpose of the present master thesis is to expand knowledge about drag and lift forces on fouled aquaculture nets. A net cage will experience angles of attack when the incoming water flow from current is not orthogonal to the twines of the net, due to the orientation of the net or the displacement. The report will describe a method for designing and executing a range of experiments related to the angle of attack and solidity, on a rigid net section with fouling. The drag- and lift coefficients for fouled nets can then be confirmed for different angles of attack and solidities. Thus, it is possible to compare experimental drag coefficients with established methods for calculating drag and lift coefficients on net panels.

The thesis hopes to answer these research questions:

- What is the best way to model a net with biofouling, for experimental testing?
- What is the difference in the drag and lift forces on clean nets in comparison to hydroid fouled nets?
- Is net panels with fouling dependent on solidity, angle of attack and Reynolds number?

In the end, this project has ambitions to point out updates needed to assure technical approval in NS9415.

1.3 Scope and limitations

The proposed topic for the present master thesis is to expand knowledge about the drag- and lift forces on artificially fouled twines. The intention is to design a model that can measure the forces on twines and net panels towed in water, at different angles of attack. The twines will be intertwined with artificial hydroids, like in the set up developed by Lader et al. (2015). The test will vary with towing speeds, solidity of the net and angles of attack. The net section will be a close representation of a fish farm net panel. A more detailed plan in the workload needed for this master thesis is described in some steps:

Firstly, some preparations are needed: a summary of the most important findings in the project thesis will be explained, and an evaluation of what is important to consider further in this master. A design must be chosen for the experiment; identification of facilities and equipment; evaluation the dimensions of frame and twines; evaluation which velocities to be tested for and which configurations; building a model with twines.

Secondly, it will be necessary to calibrate the load cell(s) that measure the drag and lift force. This is done with by checking the response of known weights on the load cell.

The next step includes executing and completing the experimental tests. First, measurements of the frame is executed for all velocities. The forces of the frame will be subtracted from the total response of twines. In addition, it is necessary to to the same for vertical and horizontal configurations. Finally, the net panels are tested for. All configurations are shifted to generate different angles of attack decided earlier, and tested for all velocities and solidities. This is a time-consuming step with many towing tests. To calculate the precision error, at least one test condition is repeated at least three times for a given velocity. A general evaluation of the uncertainties and error sources should also be commented on.

At last, post-processing of the results. Filtration of the results is done in Matlab and the representation of the relevant results. The connection between the angle of attack, the solidity of the net section, and Reynolds number is discussed. Will the research lead to a more realistic interpretation of a hydroid fouled net? A comparison between clean nets and fouled nets is needed.

The scope is limited to available testing time in the towing tank facility, schedule of the mechanical technicians at NTNU and accessible equipment.

Literature Review

2.1 The net cage

Floating aquaculture installations of salmon, are divided into categories based on their design. Classification can be done in two ways, based on the containment system or from a structural point of view. In most research regarding sea loads in aquaculture, a gravity fish farm is considered, with flexible systems. Its main shape is circular, with a HDPE floating collar a net as containment system and a grid for mooring. (Fredheim and Langan, 2009) This type of cage system is also considered in this master thesis.

The net is suspended inside the floating collar. It is important that it is rigid to retain its shape and at the same time flexible enough to minimize effects from environmental forces. Weights are connected to the net to help keep its original shape and volume at all times. (Fredheim and Langan, 2009) The netting is made from an elastic netting material, such as nylon. The small netting ropes are knitted in a pattern, usually a squared and knot less pattern, called a Raschel knitted netting, seen in Figure 2.1.



Figure 2.1: Rachel knot less knitting. (Klebert et al., 2012)

The net is often characterized by its solidity, S_n . The solidity is the fraction of pro-

jected area of the twines to the total net area. The solidity for a net panel with squared mesh is given by:

$$S_n = 2 \cdot \frac{d_w}{l_w} + \frac{1}{2} \left(\frac{d_w}{l_w} \right)^2 \quad (2.1)$$

where l_w is the half-mesh/length and d_w is the twine diameter. The dimensions which describes this net is illustrated in Figure 2.2. The solidity is a number between 0 (open net) and 1 (closed net) and usually it is between 0.20 - 0.30 for commercial netting and is adjusted for production purposes.

The flow around each twine of the net is defined by the Reynolds number, Re . Reynolds number is an expression of the inertia forces and the viscous forces in a flow and the value characterizes the flow around the cylinder or twine. For low Re numbers, the flow is laminar and viscous forces dominate meanwhile for large Re numbers, turbulent flow occurs and the forces which dominate are inertia. Re is based on the relevant twine diameter d_w , the current velocity U and the kinematic viscosity of the medium, see Equation 2.2,

$$Re = \frac{U d_w}{\nu} \quad (2.2)$$

2.2 Forces on a submerged cylinder

The net is composed by a million twines in a square pattern (Raschel). The twines can be considered as cylinders with a length l_w and diameter d_w . According to Blevins (2003), the force F exerted on a body in fluid flow will contain components both perpendicular to the mean flow (lift) and parallel to the mean flow (drag), as illustrated in Figure 2.3. The major influence on the fluid dynamic drag in this case will be the pressure drag due to separation. The drag and lift forces on a submerged cylinder is calculated by Morrisons equation. The total drag and lift forces will follow Equation 2.3 and 2.4.

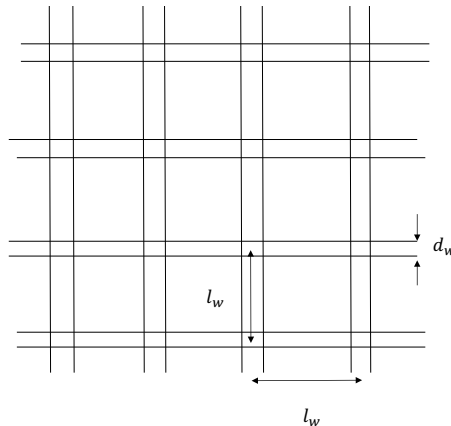


Figure 2.2: A net consisting of physical twines with a length l_w and diameter d_w .

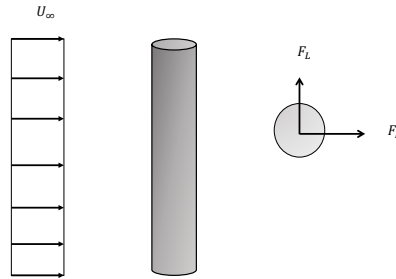


Figure 2.3: Drag and lift force on a submerged cylinder (twine).

$$F_D = \frac{1}{2} \rho C_D A U_\infty^2 \quad (2.3)$$

$$F_L = \frac{1}{2} \rho C_L A U_\infty^2 \quad (2.4)$$

where ρ is the density of water, C_D is the drag coefficient, C_L is the lift coefficient A is the area of the net panel and U_∞ is the ambient current velocity.

When the submerged cylinder is tilted and/or the velocity is incoming from an angles different than 0° , the velocity of the current and force vector is decomposed. The angle of attack is the angle between the center line of the canted cylinder and the incoming ambient current. By decomposing the current so it becomes perpendicular to the vertical cylinders, the relative current is dependent on the cosine of the angle. The drag and lift force is dependent on cosine and sinus, respectively.

2.3 Modelling of loads on a submerged net

To analyze the hydrodynamic loads exerted on a fish cage model, two methods are derived; i) Morrison type and ii) screen models. For Morrison type, the net is represented by a system of horizontal and vertical twines. The method for calculation of drag- and lift forces on the net cage, is derived on the main assumption that the total force on the net cage is given as the sum of forces acting on each twine. In this method, there are two objections. The Morrison equation is based on the cross-flow principle and cannot be justified for angles over 45° . Also, interaction effects between the twines is not accounted for. This model is reliant on the Reynolds number (Re) for evaluating the drag- and lift coefficients. The coefficients is found by rearranging of Equations 2.3 and 2.4, when the force is known.

For approach ii), the net cage is divided into several net panels, or screens. The total force on the cage is found by summing the forces on the panels. The total force is not in the flow direction due to a deflection of the flow through the screen. The orientation of the panel relative to the inflow is denoted by the angle, θ . The force is decomposed into

a lift and drag component. The force coefficients are determined by Reynolds number, the solidity of the net and the angle of attack. It is not possible to find an expression for C_D for combinations of all these parameters. An estimated functional relationship was developed by Løland (1991), by combining theoretical work and model tests on net panels and cage systems. Model test were done for various solidities, twine diameters and current velocities, and is independent of Reynolds number. The drag- and lift coefficients are found from the functional relationship in Equations 2.5 and 2.6,

$$C_D = 0.04 + (-0.04 + 0.33Sn + 6.54Sn^2 - 4.88Sn^3)\cos\theta \quad (2.5)$$

$$C_L = (-0.05Sn + 2.3Sn^2 + 1.76Sn^3)\sin 2\theta \quad (2.6)$$

where Sn is the solidity of the net and θ is the angle of attack. The relationship is valid for Re numbers ranging from 170 - 1830, solidities of 0.13 – 0.32 and angle of attack in the range of 0 - 90 °. (Løland, 1991)

2.4 Fouling of net cages

When a object is submerged in sea water for some time, it is likely that fouling organisms settle on the surface. Fouling is regarded the undesirable accumulation of microorganisms, algae and animals on structures submerged in seawater (De Nys and Guenther, 2009). A safe environment, availability of food and possibility to settle with a colony, is important parameters for the fouling organisms to chose a habitat. In the environment of an aquaculture net, it has access to all mentioned above.

Unfortunately, fouling is a danger to the fish farm. The problems can be categorized as i) it restricts water exchange by bending the flow around the net and causes lower oxygen levels in the cage (Oppedal et al., 2011) ii) it increases risk of sea lice as the delousing performance of cleaner fish drops (Blöcher, 2013) and gill health deceases is caused by hydroids directly, iii) it increases loads on the structure and increase deformations (Moe-Føre et al., 2016). The most common fouling species are the hydroid *Ectopleura larynx* (syn. *Tubularia larynx*), the mule mussel *Mytilus edulis*, the acsidian *Ciona intestinalis* and algae of the genus *Ulva* and *Ectocarpus* (Blöcher, 2013). Hydroids are found to be the most abundant fouling organism in coastal waters in Mid-Norway. They are recorded as one of the first settlers on a net cage, they also reproduce quickly and are versatile. A net fouled with colonies of *E.larynx* is seen on Figure 2.4.

A full grown *E. larynx* can be described as consisting of three body parts, as shown in Figure 2.5. The lower part is the hydrorzia, consisting of branched stolons. It is a horizontal rooting system to the attachment point on the net and to other hydroids. The middle body part is the hydrocaulus, which is the stem, erecting the hydroid. Several hydraculi can arise, made of a coenosarc (tissue overlaying the skeleton) and perisarc (outer hardened skin). This part of the hydroid is flexible, but the persiac can also snap. Each hydraculus will carry a single hydrant. The head part of the hydroid is called the hydranth if the polyp is feeding polyp or gonangia if the polyp is reproductive. Most of the hydroids in a colony have polyps specialized for feeding. It also has aboral tentacles (flexible organs far from mouth for securing food), mouth (for nutrition) and oral tentacles

(flexible organs close to mouth for securing food). (Gili and Hughes, 1995) The life cycle of hydroids are relatively fast and is completed within 24 days. First of all they grow in length, and at the same time they can reproduce themselves by budding. Budding, is an outgrowth due to cell division and it will spread through the hydroids root system. After 24 days, the gonophore development is completed and the actinula larval is released and spreads with water. Colonies of hydroids are formed, which all are anatomically and functionally connected. (Gili and Hughes, 1995)

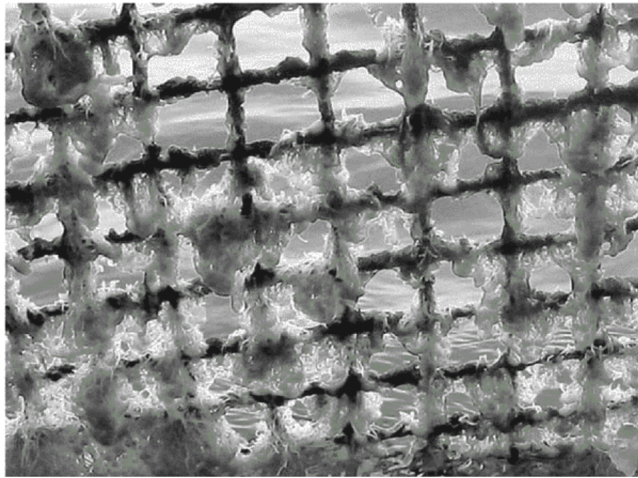


Figure 2.4: The hydroid *Ectopleura larynx* fouling a salmon net in Norway during late summer. Photograph by Leif Magne Sunde – SINTEF. Taken from De Nys and Guenther (2009).

As mentioned, *E. larynx* is known for its versatility. It has been observed that the fouling organism has three strategies to attach and remain attached to the net, see Figure 2.6. First, the hydrophytons (hydrorhizia and hydrocalus) grow around threads of the net and often intertwines, creating a firm grip around the thread. Second, the hydrophytons grow in between loose filaments of the thread. The filaments creates a strap which secures the hydroid to the net. Third, some hydroids integrates the thread filaments as part of the persiac. (Carl et al., 2011)

It is desirable for farmers to eliminate fouling from nets. NS9415 sets the requirement of a description for handling/cleaning fouling on nets, in relation to risk of fish escape. The handbook sets the actual requirements for cleaning. The antifouling strategies in Norway can be divided into three categories: copper impregnated nets combined with drying of nets, copper impregnated nets combined with washing (and drying if needed), non-impregnated nets and frequent change of nets (Olafsen, 2006). As there is no regulation regarding which method to use, each farmer can use their preferred method. The most common approach among farmers is to use a multifaced strategy to fight fouling, with copper impregnated nets in combination with washing. Copper nets only supply cover for about 6 months due to leaching and washing, and is therefore often combined. (Guenther et al., 2011) Washing of nets is carried out *in situ* by high or low pressure robotic equipment under water. The response of *E.Larnyx* to underwater washing of cage nets is

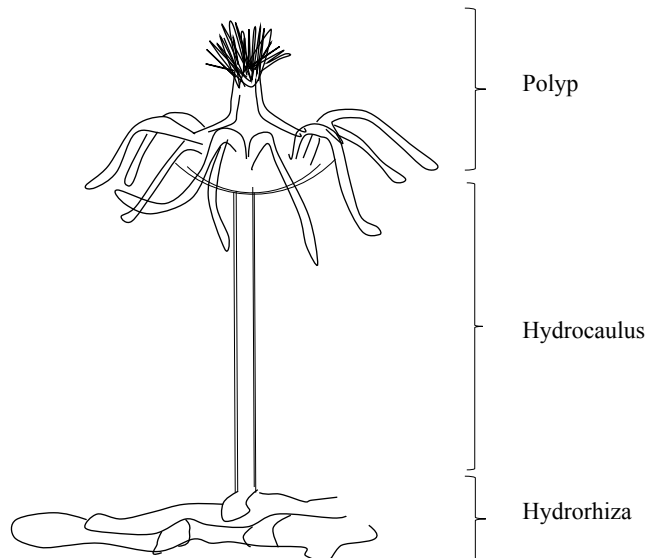


Figure 2.5: Main parts of *Ectopleura larnyx*. The illustration is inspired by Hayward and Ryland (1990).

researched by Carl et al. (2011) where samples are taken at a salmon farm in Mid-Norway. The results shows a large increase of propagates in the water during and after washing the nets. The underwater pressure creates a strong local current which spreads the propogulates in the water column and induce the gonohores to burst and release actinula. As soon as the current returns to the ambivalent velocity, the actinula will encounter available space on the cleaned net and hence settle. Carl et al. (2011) Also, cleaning does not remove all of the fouling from nets. Some organisms or just the regenerative body parts may remain on the nets. Guenther et al. (2010) This can facilitate a rapid re-colonization of the cleaned and free nets. As mentioned, hydroids have a rapid life cycle, growth and expansion by asexual budding.

Consequently, fish farmers have developed a regular scheme for cleaning. Some adopt regular cleaning every fourth-night regardless of the fouling amount on the nets. Some also clean after inspection of the fouling accumulation on the nets, resulting in intervals of around 8 weeks in the winter and up to once a week during the summer and the main fouling season. Blöcher (2013)

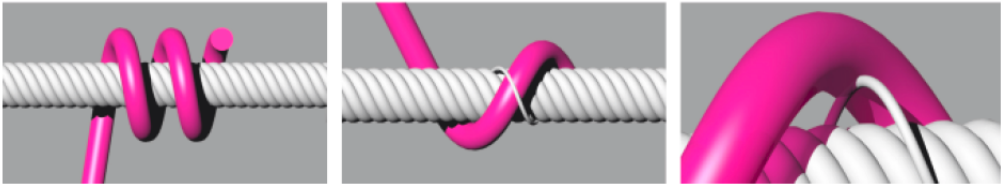


Figure 2.6: Overview of the three stages of *E. larynx* to maintain their settlement to the net. Taken from (Guenther et al., 2011)

2.5 Results from project thesis

The fouling factor is studied in a project thesis during the autumn of 2018. The background for the topic is the lack of confidence in the calculations of the drag force on nets with biofouling, used in NS9415. In chapter 8.5 it is describes that *the calculations of the net pen shall minimum include a volume of fouling which gives up to 50% increase of the twine diameter in the net pen as a whole*. The qualification for this value is not stated and is questioned from the industry. It is of interest to research if an increase in twine diameter would give the same drag forces as for artificially fouled twines, and how much fouling, in mm, the 50% diameter increase corresponds to. In the prior project thesis, experiments with artificial fouling on twines is analyzed in relation to the applied calculations of fouling on net.

In experiments executed by Lader et al. (2015), twines with artificial hydroids are towed, and the drag forces are measured. The result describes how the drag force, F_D , on two single twines with hydroid fouling increases with a quadratic and linear term, $F = AU^2 + BU$, during increased towing velocity. From this, the drag coefficients are calculated for a range of Reynolds numbers shown in Figure 2.7. The calculated C_D differs from the estimation of drag coefficient on a single cylinder found by Hoerner (1965). The effect of hydroid length, in relation to drag coefficient, is then found by using 9 mm, 16 mm and 20 mm hydroid fouling as references. The relationship is described in Figure 2.8. C_D is calculated from the drag equation with a projected area of one cylinder with length 29 mm and twine diameter of 2.9 mm.

Two conclusions can be extracted from this; the fouled twines have a Re dependant drag coefficient, while clean cylinders does not. Therefore, the difference in drag coefficients from fouled and clean twines will decrease with increasing Re . In addition, the drag coefficient on fouled twines is dependant on hydroid growth. If the twine diameter is increased by 50% like NS9415 suggests, does the calculated drag force account for the added force from biofouling? Is there a difference in calculation of drag force with Morrison type and screen type models? How much fouling, in mm, does the calculated force account for?

The drag force on a fouled net is calculated with drag coefficients from the experiment with 9 mm fouling. For Morrison type net panel, the coefficients are assumed equal to 1. For screen type, the coefficients are dependant on solidity of the net. The net panel is given a solidity of 0.205 and with an increase of twine diameter, the solidity increases to 0.31.

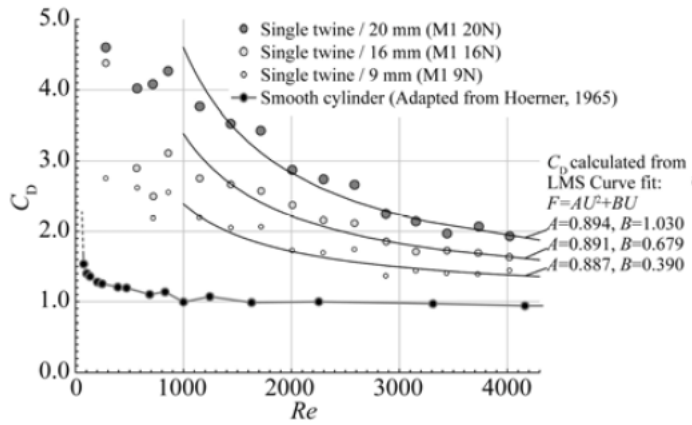


Figure 2.7: Curve fits and data points showing drag coefficient for Reynolds number and the estimation from Hoerner. Taken from Lader et al. (2015).

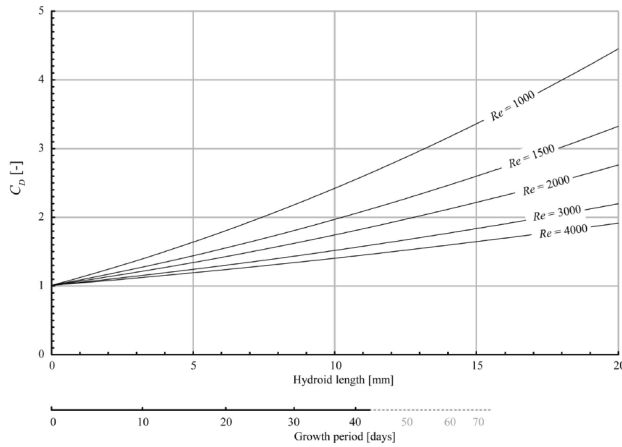


Figure 2.8: Relationship between growth period, hydroid length and drag coefficients for different Reynolds numbers. Taken from Lader et al. (2015).

The results are presented for the two given cases. The intention is to compare the drag coefficients and drag force for original clean nets, clean nets with increased twine diameter and fouled nets. The comparison is done for Morrison- and screen type models.

- Case 1: it is investigated how the drag forces are developing when the current velocity is increasing, and the fouling remains constant. The percentage difference in the forces from fouled net and clean net is calculated over increasing current velocity. This is seen in Figures 2.9 and 2.10, for hydroid length of 9 mm. As the current is

increasing, Morrison type net panel with increased twine, gives same drag forces as fouled nets. The drag force from screen type models are too low.

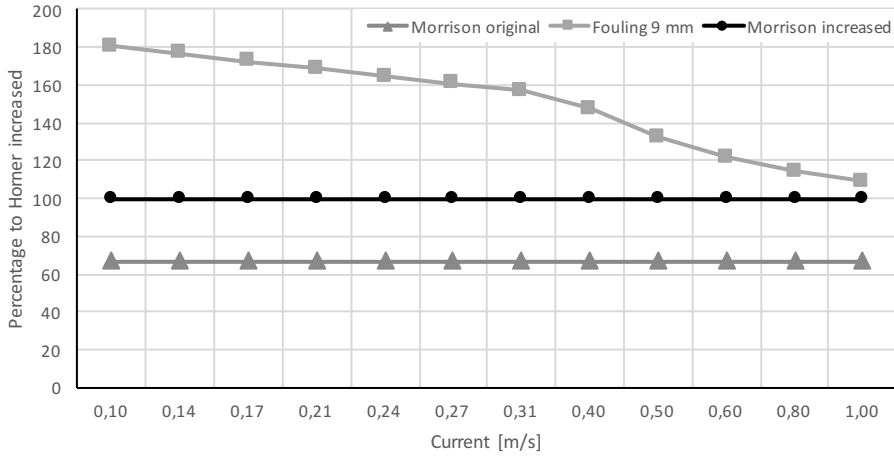


Figure 2.9: Percentage difference to Morrison type increased drag force

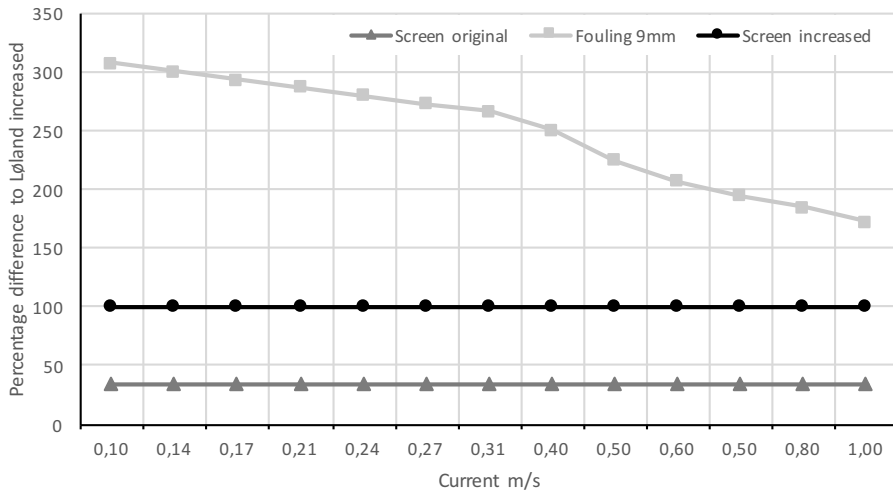


Figure 2.10: Percentage difference to screen type increased drag force

- Case 2: it is investigated how the drag forces develop when the current is constant, and hydroids are growing in length. When Re is 1000 and 3000, the result obtained is presented in Figures 2.11 and 2.12. The estimated drag force using Morrison method and an increased twine diameter, corresponds to a drag force at 3.5 and 10.5 mm fouling, respectively. Screen type calculation, with increased twine diameter, gives very low drag force results.

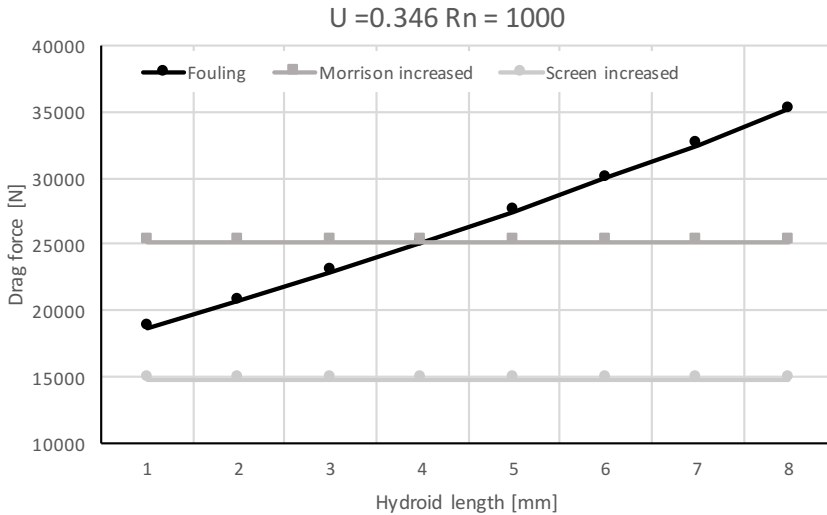


Figure 2.11: Intersection of drag forces for a constant current velocity 0.346 m/s

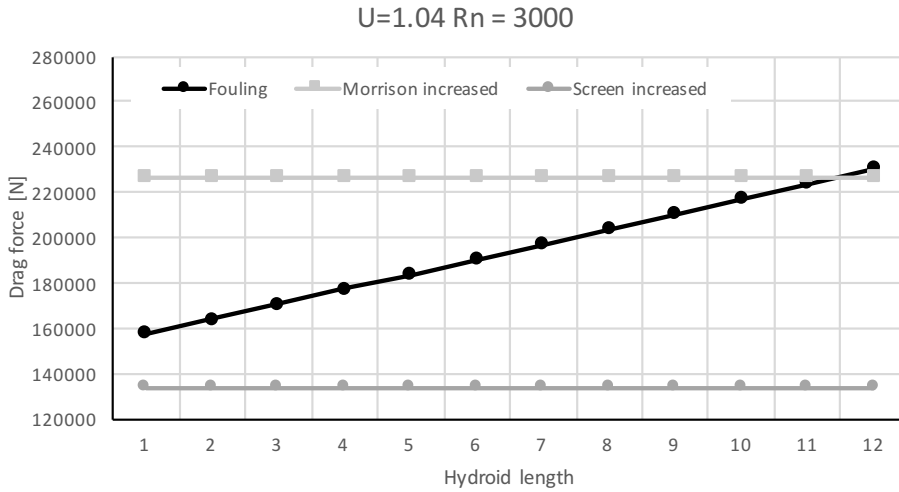


Figure 2.12: Intersection of drag forces for a constant current velocity 1.04 m/s

Conclusion

For a constant hydroid growth of 9 mm, Morrison method with increased twine will under-predict drag forces at low velocities. As the velocity increases, the forces coincide. This is due to the behaviour of hydroids in current, they bend and become more streamlined, creating a lower drag coefficient. The dimensioning current velocity by national standards is above 0.5 m/s and eliminate most of this issue. The drag force on clean net panels calculated by screen model, with increased twine, is not a good estimate for drag force on fouled nets. It underestimated the forces by 3 to 1.5 times.

Hydroids in strong current gives less C_D than for slow, due to the streamlining of hydroids. The higher the dimensioning current, the higher tolerance for the hydroid length. From the results, it is suggested that for higher dimensioning current velocities (at high Re), it will not be necessary to add 50% of the twine diameter to account for fouling, but a smaller value.

Further work recommended from the project thesis is to investigate the effect on drag for different solidities and angle of attack. Also, the coefficients tested for are based on single twines and not pet panels. A screen type model with fouling will be more accurate. Experimental tests with net panels are therefore also recommended.

2.6 Experimental testing

To develop reliable methods for current force calculation, one is to a large extent dependent on model tests. The model test give important information about physical effects, and data are sampled for validation of the theoretical model. (Løland, 1991) It is known to use both numerical and experimental testing to predict loads on aquaculture installations. Experimental testing is mostly used to validate numerical models. In cases where the results differ, the experimental results are considered the "right" values, if not too much uncertainties lies behind the results.

Regarding drag forces, Gansel et al. (2015) indicated that two techniques for drag measurements of a net are available: i) the net is placed in a tank large enough to avoid any wall effects and ii) the net spans almost the entire cross section of the tank. When adding hydroids to the nets as well, two approaches are developed i) sample hydroids from growth on net panels immersed in sea water ii) create artificial hydroids attached to twines. The weakness of the first approach is that some hydroids will die in the transition from seawater to a fresh water tank. Most hydroids will loose their "heads". The weakness of ii) is that a lot of simplifications are done to model the artificial hydroids, such as diversity in lengths, thickness, density and size of the "head".

In cases with net panels, scaling of the net panels is not performed. All models have a scale ratio of 1:1. This is to ensure that the Reynolds number effects are theoretically matched. The flow will then behave in the same way for model and full scale and the drag forces can be scaled for a larger panel.

For this master thesis, it has been evaluated to continue with a model where i) a net panel is placed in a tank large enough to avoid any wall effects and ii) create artificial hydroids attached to the twines in the panel. The twines must be non-elastic to measure the forces exerted on them. The twines configured as a net panel, must be kept in place by a construction, such as a frame. Also, the frame must be able to rotate about the Z - axis to generate different angles of attack. The frame with twines can be towed in the tank. A preliminary design is illustrated in Figure 2.13.

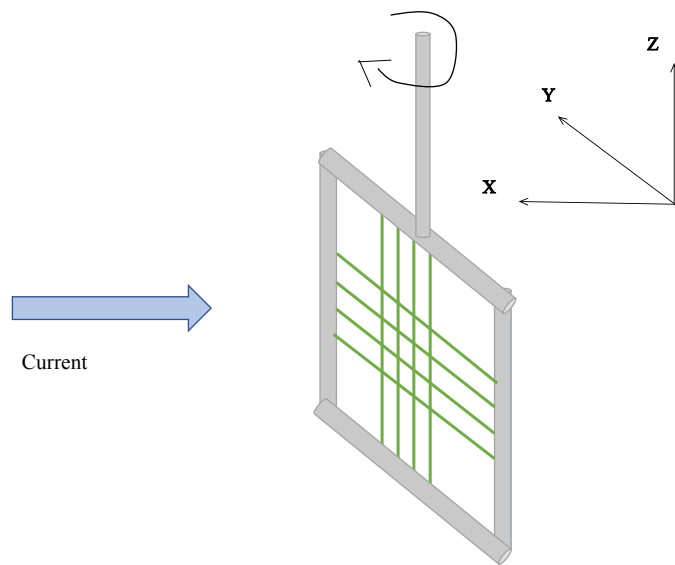


Figure 2.13: Preliminary set up for experimental testing

Method

3.1 Pre-experiment

3.1.1 Flow disturbances

It is important that the wake behind the cylinders of the frame does not disturb the incoming flow on the twines. The velocity of the flow entering the twines is then altered, in addition to a slight change in the angle of attack. As the rotation of the frame around the Z- axis increases and Re increases, the wake of the vertical cylinder frame is in position to interfere with the streamlines encountering the twines. The vertical twine closest to the frame is exposed to this risk and the artificial fouling reach even closer to the wake of the frame.

When the flow encounters the frame, it will eventually separate at the rear. The separation is due to the balance between inertial forces and viscous forces. Reynolds number expresses the relative importance of forces and describes the flow pattern for different regimes. The vertical part of the frame consists of circular cylinders and have Re numbers of 5000 - 25000, which gives a laminar separation with a turbulent vortex street. In this subcritical area, the flow separates at 80° downstream from the stagnation point and the vortex shedding is turbulent. The width and length of the wake are estimated by finding the distance of which the disturbed flow returns to the incoming velocity. A dipole in a parallel stream gives the streamlines around a cylinder. (Pettersen, 2018) The velocity distribution over the cylinder in cross-flow is given by Equation 3.1,

$$U_\infty = \sqrt{u_\theta^2 + u_r^2} = (-U_\infty(1 + \frac{a^2}{r^2})\sin\theta)^2 + (U_\infty(1 + \frac{a^2}{r^2})\cos\theta)^2 \quad (3.1)$$

where U_∞ is the velocity far upstream of the cylinder, a is the cylinder radius, r is the radial coordinate from the center of the cylinder and θ the angle measured from the forward stagnation point. The velocity at 90° , orthogonal to the current direction, will have maximum velocity and at 180° , behind the cylinder, the velocity is at a minimum. Considering a radius of the cylinder frame to be maximum 19 mm and a maximum velocity of

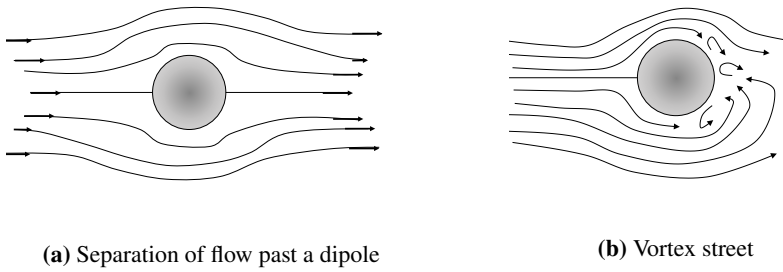


Figure 3.1: Different flow regimes past a circular cylinder. Illustrations are inspired by Sunden (2011)

0.6 m/s, the velocity of the streamlines will return to 99.93% of incoming velocity at $1r$. The exterior twines must at all times be at a distance of 0.019 m, 1.9 cm, from the cylinder frame. Due to the simplification of the calculation method, a minimum distance of $2r$, 3.8 cm is set. In Figure 3.2 this is illustrated as the angle increases and the distance d is calculated in Table 3.1.1. See Appendix for calculation of the velocity of the streamlines.

Theta [°]	0	10	20	30	40	45	50	55	60
Distance d [cm]	3.8	3.85	4.04	4.38	4.96	5.37	5.91	6.52	7.6

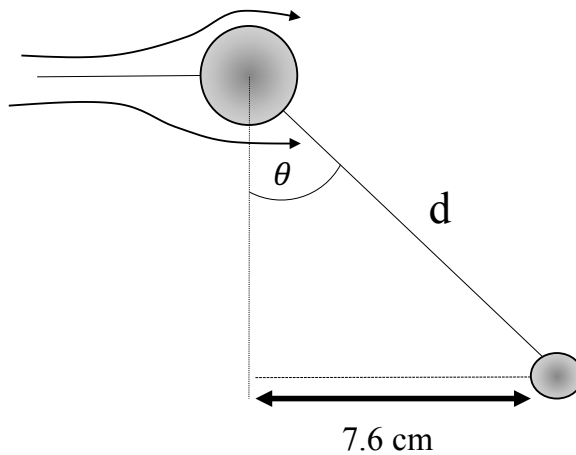


Figure 3.2: Illustration of the distance d , seen from above.

3.1.2 Conceptual choices

The experiment is designed to have three variables; velocity, angle of attack, and solidity, summarized in Table 3.1.2. Solidity usually ranges between 0.2 and 0.3 in the industry

and with three data points between this interval for solidity it is possible to find a trend in the results. The area of the net panel is fixed and varied with 16, 14 and 12 twines to create different solidities. Angles of attack are chosen based on the flow disturbances and five different angles are chosen to give a variety of results. The towing velocities are determined based on the features of the towing wagon, and previous experiments. Experiments done by Lader et al. (2015) with low velocity had to be discarded due to inaccuracies with the towing wagon. The towing wagon at NTNU has the possibility of very low velocities, with high reliability. Therefore, it will be tested for low velocities in this experiment. The wake will not inflict on the twines with the chosen angles and velocities, as the twines are placed in the middle of the frame, at 322 mm from the cylinder frame.

Half mesh [mm]	22.0	26.2	32.0			
Solidity	0.28	0.24	0.19			
Panel of twines	8x8	7x7	6x6			
Angles [deg]	0	15	20	20	45	
Velocity [m/s]	0.05	0.1	0.2	0.25	0.3	0.35

Table 3.1: Parameters for the experiments

The constants in the experiment are; the diameter of twine, length of twine, the density of artificial hydroids on twines and hydroid length, summarized in Table 3.1.2. The dimensions are based on previous research from Lader et al. (2015), where net panels are immersed over three and six weeks. That resulted in hydroid growth with an average stem thickness of 0.29 mm and a density of 1.4 hydroids/mm of a twine. The average length is influenced by the immersion period and varies between 6.4 to 11.2 mm. In this thesis, a 0.26 mm multifilament spectra fishing line made of nylon is chosen to model the hydroids. The fishing line has a thread diameter similar to the measured diameter of the hydroids. Similarity in the stiffness of the real and artificial hydroids is also important. There is no available data on hydroid stiffness, only samples left from the experiment by Lader et al. (2015). In the study it is discussed how the stiffness of the nylon thread compares to real hydroids. It is qualitatively assessed this by visual observation of the behavior in water, and there is no indication that this thread behaves differently from the live hydroids. For this master thesis, a line with breaking strength of 24 kg is evaluated, but it is too stiff. The next similar thread had a breaking strength of 15 kg which is much more flexible. The specifications of the thread is found in Appendix 3.2.2. The length of the artificial hydroid threads is 16 mm. This value is chosen for means of comparison to other experimental tests, like Lader et al. (2015). In addition, it represents a growth period of 60 -70 days for hydroids, which is an absolute maximum length. As mentioned, cleaning cycles are most commonly done every fourth-night, but can go up to 8 weeks (56 days).

To model the core of the twines, steel rods are twisted with the fishing line placed in between. This will simulate the attachment as described in Section 2.4. Since the dimensions of fouling are similar to the live specimen, the scale ratio is 1:1. The twine diameter must also correspond to a normal twine diameter found in aquaculture nets and is chosen to be 3 mm. The length of the twines is 500 mm and the net panel then 500 mm x 500 mm. Here, the *net panel* describes the inside of the frame, while *net section* is only

the area of twines crossing.

	Twines	Fouling
Diameter [mm]	3	0.26
Length [mm]	520-540	16
Density [hydroids/mm]	-	1.4

Table 3.2: Constants used for the models

The artificial hydroids are evenly distributed with a density of 15 hydroids per cm, and a thickness of 0.26 mm. The length of the artificial hydroids is 16 mm. The values are based on average measurements from hydroids growing on aquaculture nets. Both Lader et al. (2015) and Sæther (2015) have done several experiments on twines with this density, thickness and hydroid length and the new research can be put together with this.

3.1.3 Expectation of forces

The expected drag- and lift forces on the model frame and twines is calculated pre-experiment. The intent is to find maximum and minimum forces for selection of a suitable load cell. Since the twine models will be made of stiff materials, the projected area will remain the same and the calculations will give a good estimate of the exerted forces. Drag forces on a panel are calculated using a Morrison type approach where the exposed area is assumed to be constant and the front of the twine has no shielding effects on the rear side. The projected area of the frame is also included in calculations, with expected values of the diameter.

Current velocity on a net panel with an incoming current at different angles gives decomposed current and force vectors. For horizontal twines, the lift force is zero and the drag is not affected by the angle. For a vertical twine, the result is as illustrated in Fig 3.3. The normal force, F_N , is directed normal to the twine. The normal force includes a decomposing of the ambient current. The drag force, F_D , is in the direction of the ambient current inflow. The lift force, F_L is orthogonal to this. The total drag- and lift forces are described in Equations 3.2 and 3.3. The largest drag forces on a net occur when the angle is 0° (current is orthogonal to twine) and the largest lift forces occur for an angle of 45° .

$$F_D = \frac{1}{2} \rho C_D A U_\infty^2 (\cos\theta^3 + 1) \quad (3.2)$$

$$F_L = \frac{1}{2} \rho C_L A (U_\infty \cos\theta)^2 \sin\theta \quad (3.3)$$

The total drag and lift forces are measured in X and Y - direction. For a fouled twine, drag coefficients from experiments by Lader et al. (2015) are used, which is 3 at maximum Re . For the clean twines and the frame, drag coefficients are based on spheres where C_D is 1. For lift coefficients of fouled twines, coefficients are unknown. For lift coefficients on clean twines and the frame, coefficients are based on spheres where C_L is 0.3. Minimum and maximum forces are calculated from only frame and frame with 8 vertical and 8 horizontally fouled twines, respectively. Expected drag forces range between minimum

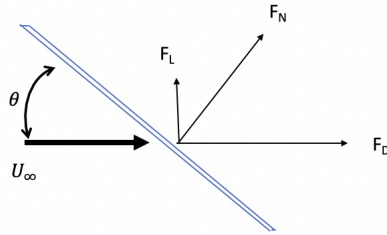


Figure 3.3: Two dimensional illustration of decomposed forces on a vertical twine with arbitrary orientation in a Morrison type force model. $F_N = \frac{1}{2} \rho C_D A (U \cos \theta)^2$

0.27 N and maximum 9.33 N. Expected lift forces range between minimum 0.02 N and maximum 0.39 N. Two strain gauge transducers with 18 kg measurement is chosen. Load cells of 18 kg are the smallest available at NTNU. Ideally, a load cell for smaller forces should be installed in Y-direction, due to the very low expected forces. It is chosen to use two of each load cell, to make sure the frame is stable enough. Vibrations in the frame and bending moment are not wanted.

3.2 Production of model

3.2.1 Frame

When the dimensions for the whole models are set, the lab technicians at NTNU produced model drawings of the setup. It included a frame to mount the models, four load cells holding the model frame connected to the back frame, the back frame attached to the wagon and a steering device for controlling the direction of the model frame. The model is seen in Figure 3.4 and is an improvement of the preliminary model. The waterline is placed 10 cm above the frame clamping the twines. The materials used for the frames that are not submerged is made of parts remaining from other projects. Most parts are square aluminum profiles, welded together. The drag on the submerged model frame should be low compared to the forces on the twines and at the same time be stable during towing. Thus, it is made of circular and elliptical shaped cross-sections. The vertical parts of the frame is made of cylinders with a diameter of 38 mm and the horizontal parts are made with elliptical shaped steel with a cross-section of 30 x 13 mm. Elliptical profiles are chosen as they are streamlined, will minimize drag and does not irrupt the flow. The vertical parts cannot be made of elliptical profiles, due to the increased lift when the frame rotates, and therefore a circular cross-section is chosen. On all sides, the profiles are split longitudinally. The loose section is 220 mm. The part that is cut off is connected to the frame by two screws, creating a clamp to fasten the twines. The shape of the profile is still the same and the incoming flow is not altered, as the screws are situated at the back.

A cylinder is welded to the frame, with another cylinder inside with a bearing. On top of the rotating cylinder, a print-out a protractor is put on a disc, to set the angle of attack.

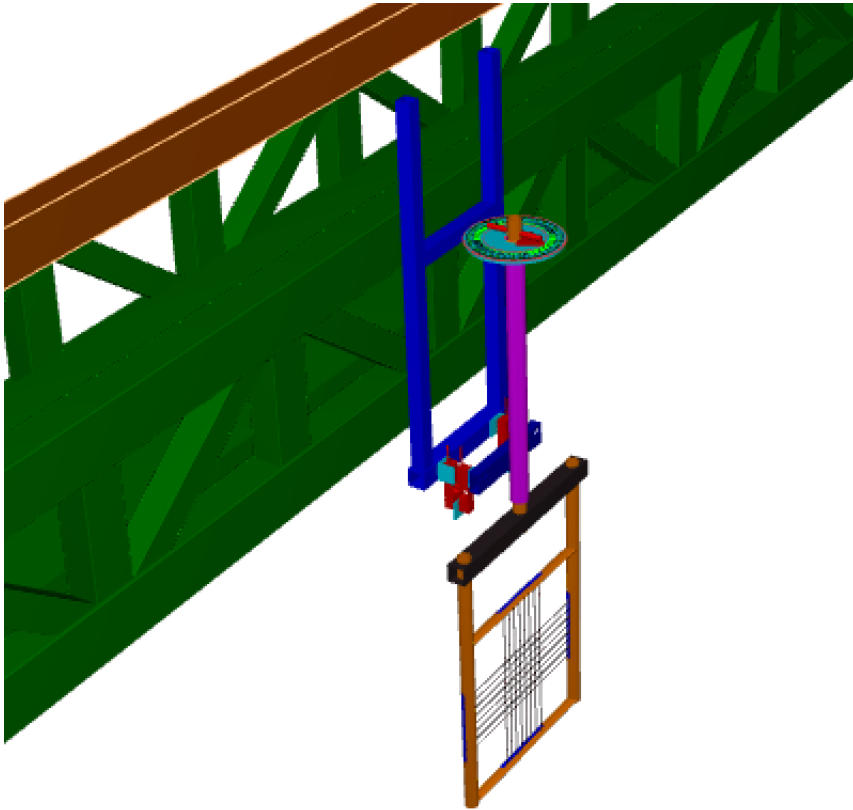


Figure 3.4: The towing wagon(green), back frame(blue), front frame(orange), rotating device (pink) and twines

3.2.2 Clean and fouled twines

Recall that this study intends to continue developing research results for fouled aquaculture nets. Some work is already done within this area, and hence the methods for executing this experiment are quite similar. This is done with the intent to compare results and draw conclusions. The twines are made from two twisted steel rods with multifilament fishing line acting as hydroids, trapped in between the rods. This method was presented by Lader et al. (2015), after inspiration from industrial testing tubes.

The steel rods are commonly used for welding and are quite flexible. When twisted, they are reinforced and will not bend when exposed to current. Even though a nylon net is highly flexible, it is essential for this experiment to keep the net of twines fixed, so that the flexibility will not affect the drag measurements. The rods have a diameter of 1.5 mm and after twining, the diameter is approximately 3 mm. The models are twisted with one turn per 12 mm, like Lader et al. (2015) and Sæther (2015). While twisted, the rods counteract and the finished model is shorter. The contraction is around 5%. The rods are cut into pieces of 70 cm, with 64 cm as a working area for twisting, giving a 60.8 cm twisted

model. That results in 50.67 rotations per twine. The twisting is done with an electric drill and counted manually. A yellow marker on the drill is placed on the drill to increase the reliability of counting the turns. Figure 3.6a illustrates the process. Finally, the twines are cut into pieces of 52 cm or 56 cm, leaving 1 cm on each side for attachment on the elliptical profiles and 3 cm for fastening on the cylindrical profiles. The twines fit inside the front frame (see Figure 3.4), with fastening on the sides of the frame.

The process of making the artificial fouled twines is time-consuming and requires some trials and errors. In the end, a pipe of 35 mm circumference (11.4 mm diameter) is used to efficiently produce twines hydroid of approximately 16 mm on each side of the rod, and 2 mm cut away for the "heads". The pipe is split longitudinally with a 2 mm trail for one steel rod. The pipe and rod are then fastened to an electric drill. While the drill spins, the fishing thread is spun onto the pipe and rod, see Figure 3.5a. Since the rods counteract, 526 mm is covered with thread before twisting, to achieve a 500 mm area of fouling. To keep the density of 15 hydroids per cm (750 hydroids per 500 mm), a marker with 1/16 inch, 1.8 mm is taped on. The correct distance is 1.4 mm per hydroid, but it is not possible to find a marker with this distance. While the thread is spun, it is still possible to adjust the space. Random density tests are carried out after completion of the twine, and the density appears to be 13-15 hydroids per cm. A thin stripe of sealant is used to connect the rod, thread and a new rod on top, seen in Figure 3.5b. A handheld burner is used to cut the threads midway, leaving 16 mm on each side of the rod. While cutting the thread, small "heads" are created at the ends. They are not more than 1-2 mm thicker than the thread itself. The rods are tied together and kept overnight to let the sealant dry. After, the rods are twisted with the drill, as seen in Figure 3.5b. For more specification about the equipment used, see Appendix 5.4. The finished models can be seen in Figure 3.7

To fasten the twines inside the frame, a clamping arrangement is made by longitudinally splitting the horizontal and vertical parts of the frame. The loose part is then attached to the body with two screws, as seen in Figure 3.8. The elliptical shaped parts are solid while the circular pieces needed to be filled at the calming point, and rubber material is glued on the inside, to keep the fastening secure.



(a) Thread spun around tube and rod



(b) Thread cut and steel rods glued

Figure 3.5: Creating the artificial fouling

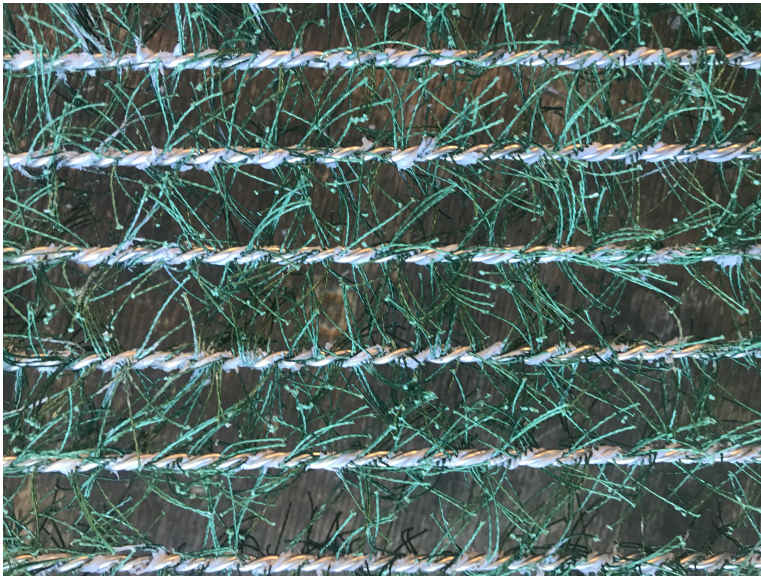


(a) Drilling of clean steel rods

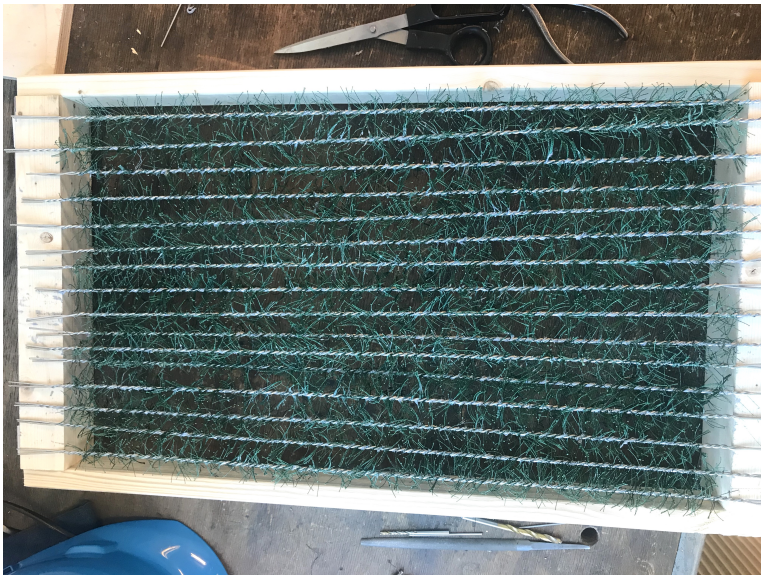


(b) Drilling of steel rods with fouling

Figure 3.6: Drilling of twines



(a) Close up of the hydroid models



(b) Full scale hydroids

Figure 3.7: Models of twines with artificial fouling



Figure 3.8: Clamp fastening frame

3.3 Assembly

3.3.1 Calibration and data acquisition

Calibration is done at SINTEF laboratories for calibration. It is executed to relate the voltage of the transducer to a physical quantity of interest and get reliable measurements. Known weights are used to find the relationship between physical quantities. In this case it is used weights of 0.1 kg, 0.3 kg, 0.5 kg, 1 kg, 2 kg and 3 kg. The weights are anchored about 40 cm below the load cells, in z-dir, seen in Figure 3.9. The distance from the load cells to the weights on the model frame gives a bending moment. For higher loads above 30N, it is difficult to get an accurate result, as the bending moment had too much influence. The calibration factor is found through linear regression of the voltage output and the force. The calibration factor is then used as input in the recording software.

The calibration is executed when the load cells are fixed to the model. Alternatively, the load cells could be calibrated beforehand. The sensitivity might have changed when mounted and therefore it is preferential to do it after mounting. Four 18 kg load cells are fixed to the frame. Even though very small forces are expected, four load cells are necessary to stabilize the frame by making it stiffer and therefore restrict unwanted vibrations as much as possible.



(a) X - direction



(b) Y - direction

Figure 3.9: Calibration of frame in lab

As the designed structure is towed along the tank, the voltages from each load cell are measured, in addition to time, position(x) and speed. The analog voltage signals will first go through built-in amplifiers, filters, and an A/D converter in an MGC+ amplifier. A 200 Hz sampling frequency is used and a low-pass filter with a cut off frequency of 20 Hz. The sampling frequency, along with the length of records, will determine the data storage. Since no higher order loads will be measured, data storage is not a dispute. The

low-pass filter is 1/10 of the sampling frequency, as often recommended to avoid Nyquist phenomena (Steen, 2014). The low-pass filter removes any non-physical effects (noise) with high frequency. The MGC+ amplifier has a range of ± 10 V. The values within this range are accepted and if values become too large it will cause an error in the system. The resolution is at 20 bit, giving 4096 values to choose from. The signals are saved by the recording system catmanAP V4.2.1. To save the total drag and lift, a channel is created for both directions containing signals and the calibration factor, see Equations 3.4 and 3.5. The speed of the carriage is controlled by a different software called MCL Carriage Control.

$$xForce[N] = \frac{8538signal}{407} + \frac{8534signal}{293} \quad (3.4)$$

$$yForce[N] = \frac{8537signal}{411} + \frac{8333signal}{301} \quad (3.5)$$

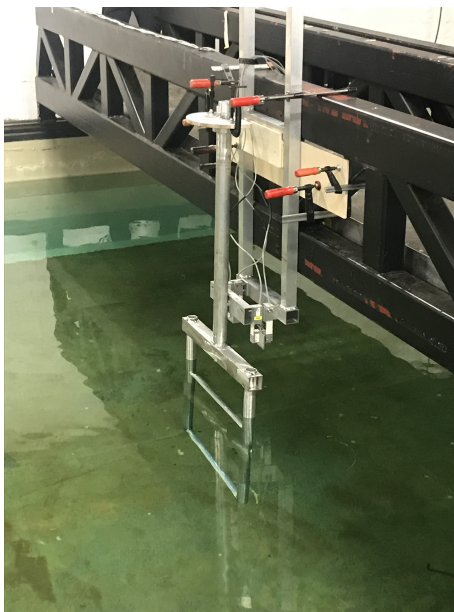
The design of the transducers is done with help from lab technicians. They are mounted as the connection point from the back frame to the front frame (see Figure 3.10a). This way, the load cells carry the weight of the front frame submerged in water and the rotating wheel on top. They are connected 15 cm above the waterline. The forces are measured more accurately when the load cell is close to the water. On the other hand, this leads to reduced stiffness of the system. The transducers are tailor made to measure force in one direction only.

3.3.2 Setup

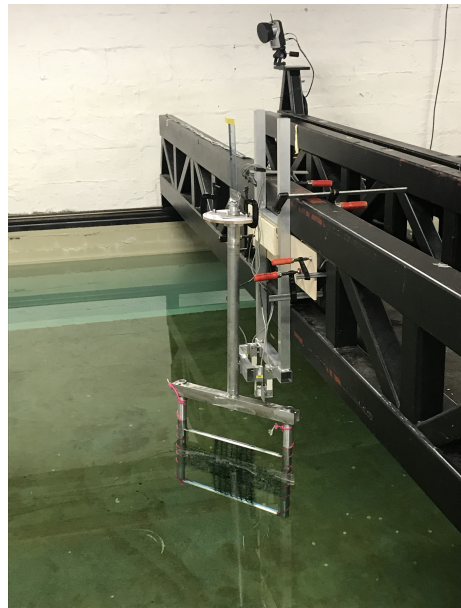
The experiments are conducted in the Marine Cybernetic lab (MC lab) at NTNU in Trondheim, Norway. This lab has many measurement abilities, but the important function in this experiment is the towing carriage. By towing the model at a specified speed, the current velocity is simulated. The main dimensions of the tank is $L \times B \times D = 40\text{m} \times 6.45\text{m} \times 1.5\text{m}$. (NTNU, n.d)

The finished model is quite heavy but can be lifted by one person by sliding it on the towing wagon. The frame is lifted from its fastening and above water level when the twines are rearranged or changed and replaced. To always make sure the frame is put into the same position, a wooden plate and block are clamped on to the towing wagon. The back frame hangs on to this plate. The towing wagon, frame, and fastening are seen in Figure 3.10a.

To avoid VIV, a rope of 5mm diameter is spun with a climb of 5.5 cycles per 50 cm around the vertical cylinders and the bottom of the cylinders are taped to restrict water exchange, seen in Figure 3.10b. The vibrations are then monitored by positioning an underwater GoPro camera at a 2 m horizontal distance from the frame.



(a) Only frame setup in lab





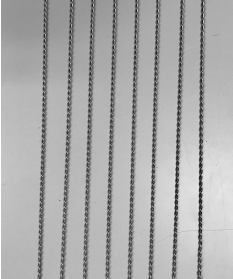
(b) Frame with VIV reducing rope and fouled net, at an angle

Figure 3.10: Setup

3.4 Experiments


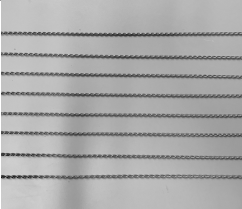
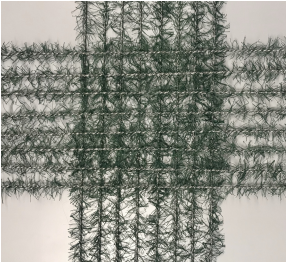
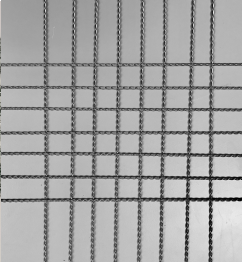

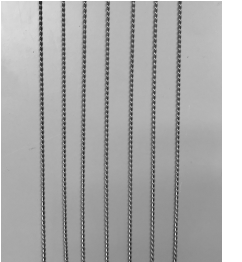
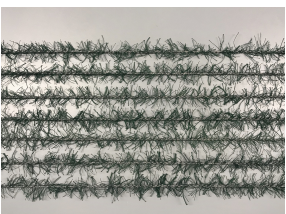
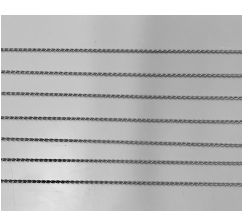
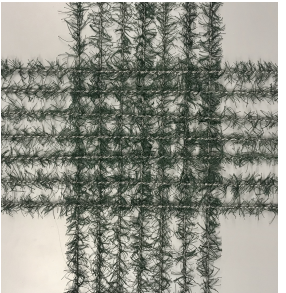
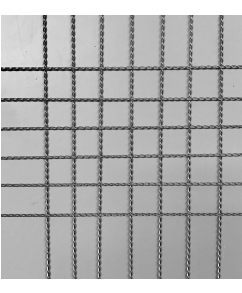
The main goal with the experiments is to achieve results of the drag and lift forces on a net section only, at low Re values with the current incoming at different angles of attack. Both the frame alone, vertical and horizontal twines had to be tested for, to accurately calculate the forces on the panel. It is not certain that the drag force acting on eight vertical twines is the same as the drag on a single twine x 8. Therefore, the frame alone and 9 twine configurations are tested for with clean and fouled twines, summarized in Table 3.3. The proposed plan started with testing of the frame alone, then all configurations of clean twines and lastly all configurations of twines with biofouling. The scheduled time included time for mounting, calibration, running tests, adjusting angles, changing of configurations and other unexpected work. In total, the expected program is 34.75 hours, which is 4.34 working days (8 hours) and the tank is booked for 1 week. Problems regarding the availability of mechanical technicians resulted in a delay in testing. The setup and simple testing on day three resulted in recalibration of the load cells. On day 4, the first acceptable test is carried out. The test did not follow the original program due to uncertainty about the availability in the tank during weekends, but luckily all tests are completed.

The spacing between the twines is a measurement for the solidity of the net section. The spacing is a measurement of the half-mesh, the distance between the twines (not center). It is set to 22 mm for 8 twines, 26 mm for 7 twines and 32 mm for 6 twines.

Biofouling	Clean	Name	Nr. of twines	Spacing	
			frame	0	0
		8-vert	8	22 mm	


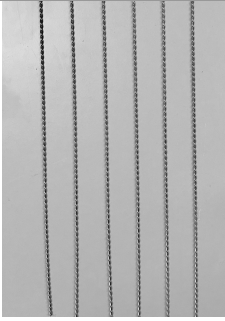

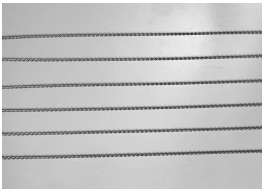
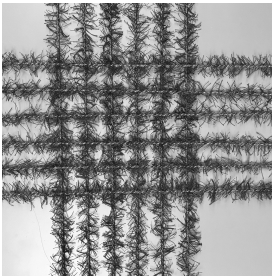
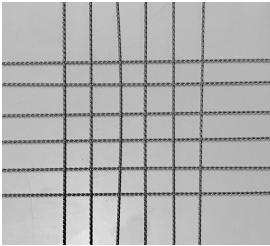
Continued on next page

Table 3.3 – continued from previous page

Biofouling	Clean	Name	Nr. of twines	Spacing
		8-hor	8	22 mm
		8-net	16	22 mm
		7-vert	7	26 mm
		7-hor	7	26 mm
		7-net	14	26 mm

Continued on next page

Table 3.3 – continued from previous page

Biofouling	Clean	Name	Nr. of twines	Spacing
		6-vert	6	32 mm
		6-hor	6	32 mm
		6-net	12	32 mm

During the first towing tests it is observed that the frame is vibrating back and forth, especially at high velocities. The wake is larger than expected due to this and VIV reducing measures are implemented. Two ropes of different diameters are tested by spinning it around the cylinders of the frame. The rope with the largest diameter showed the best result for reducing the vibrations. Still, the vibrations are present at the bottom of the submerged frame at an amplitude of about 0 - 1 cm. This is documented with a GoPro camera. It is clear that when the carriage does not keep an even distribution of velocity, but rather sporadically creates an extra pull. The construction attached to the carriage is affected by the pull. The vibrations are most likely a consequence of the twitching. For the smallest velocity runs, the twitching gives the most response and takes longer to die out. Between the twitches, the frame appears to be going steady, for all velocities. Video files for this are found in the video files in the digital attachment. From visual observation during towing tests, the wake did not interfere with the twines.

It is not expected to wait for the water to settle in between runs. For large speeds, it is often necessary to include waiting time for the waves to fade and reduce disturbance in the water. No waves developed during testing and while towing the structure slowly into

position in the tank, the water became still.

The structure is lifted from the water to change the configurations and this operation could potentially affect the sensitivity of the load cells; therefore, the load cells are calibrated with a zero measurement every time it is lifted. This is done using built-in software while the towing wagon stands still for about 30 seconds.

To estimate the precision error of the experiments, some of the configurations are repeated three times each. Due to limited testing time, it was not possible to run more tests. Ideally, multiple configurations and speeds should be tested for. In addition, decay tests in water are executed and described in detail later in this chapter.

3.5 Post processing

3.5.1 Analysis

439 runs are completed for this master thesis, which resulted in 246 binary data files. All post-processing of these data files is done using Matlab. The binary files are imported and read via the `catman` function. The analyzing could then be automated and the process of analyzing the files is more time efficient.

The method for analyzing the files is described as two main steps: 1) time-domain visual analysis of the data 2) frequency-domain visual analysis of the data. The first step is a global assessment of the validity of the tests and give a manual estimation of main forces. The second is a spectral analysis and contributes with an estimation of noise level, design of possible filtering and checking filtering results.

For the time-domain visual analysis, the first step is to detect the relevant time windows for each velocity. The towing tank has a distance of 21 m and it is time efficient to increase velocity along with the tank. For a set of six velocities (0.05, 0.1, 0.2, 0.25, 0.3, 0.35), three files are created. The files are called `v012`, `v34` and `v5` to give information about the speeds. From Excel spreadsheets, the filename, description, and interval for each run with velocity increase, is imported to Matlab. When time vs position and speed, and time vs force are plotted, the intervals are corrected by visual inspection. The transient phases are eliminated and the steady state is found. This process could not be automated, as the time intervals have different total time for each run, varying from a minimum 15 sec to a maximum 60 sec. As seen in Figure 3.11, the steady state is achieved shortly after the set speed is achieved and remains constant. The intervals are further used for calculation of total mean forces and standard deviation of drag and lift force, using built-in functions in Matlab. The data is proposed cleaned, which will remove the largest outliers seen in the time series. After a recommendation from professors at NTNU, the average force is calculated from the original signal. (Savio, 2019)

For the lowest speeds, the force measurements are very sensitive. It is noticed that for measurements of drag and lift on the frame only, a speed of 0,05 m/s gives negative values. Also, for lift measurements at 10° angle of attack, all measurements are negative.

The frequency-domain analysis can give an estimation of noise. Here, the noise level of the results is already filtered by analog low pass filter before processing and the level

of vibrations is estimated by the window error. As seen in the time domain analysis of the forces (Figure 3.11), the drag and lift forces are oscillating around a mean value. The oscillations are due to vibrations in the structure, which most likely is caused by twitching in the carriage, or flow instabilities. This is very common in standard ship resistance tests done at NTNU/Sintef and the average value from a time series with a lot of oscillation is still very reliable. This is because the vibrations are zero average components on an integer number of periods. On short time series with large oscillations, the time windows should be chosen so that an integer number of periods of the lowest significant frequency is encompassed by the time window for the average. The time windows with the steady state can be checked for errors depending on the mean force, estimated amplitude of sinusoidal oscillation on top of the average, the significant frequency of the oscillations and the length of the time window. A power spectral density plot (PSD) of the signal is created to find the frequency of the oscillations. Figures 3.12 and 3.12 show that the window error has a hyperbolic decaying and the absolute and relative windowing error is estimated. If the error is significant, the time window should be adjusted. Not all the time intervals are tested for windowing error, but the two examples provide a good estimate as they are extreme values of t_s . For the worst case, the length of the time series is 15 sec, and the relative error is 0.0137. For a much longer period where t_s is 33 sec, the relative error is given as 0.0068.

The PSD is created by using the Fast Fourier Transform (fft) function in Matlab. It gives the frequency components of a signal. The lowest significant frequency is used for calculating the windowing error.

This method is applied to all configurations, such as the frame alone, frame with clean twines and frame with twines biofouling. Excel spreadsheets are created to easily import all information needed to Matlab. The spreadsheets and Matlab-codes are found in the digital attachments and a full list of them is in Appendix 5.5.

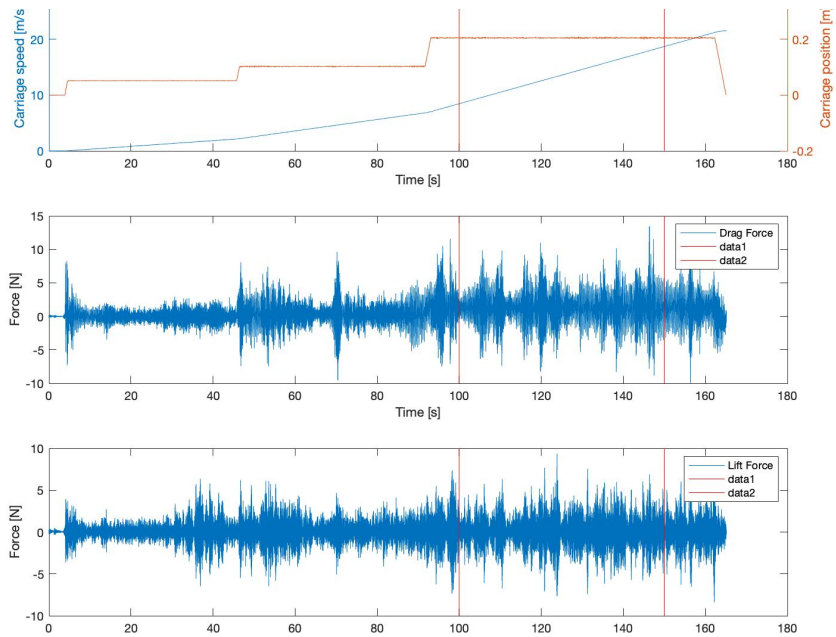


Figure 3.11: Cut interval in frame timeseries

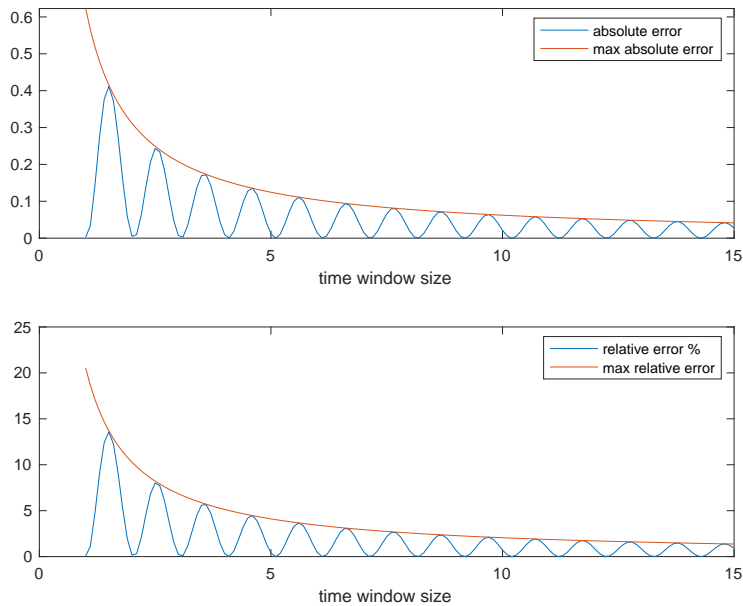


Figure 3.12: Window error when $c = 3.0325$, $a = 2.7115/\sqrt{2}$, $f = 0.98$, $t_s = 15$

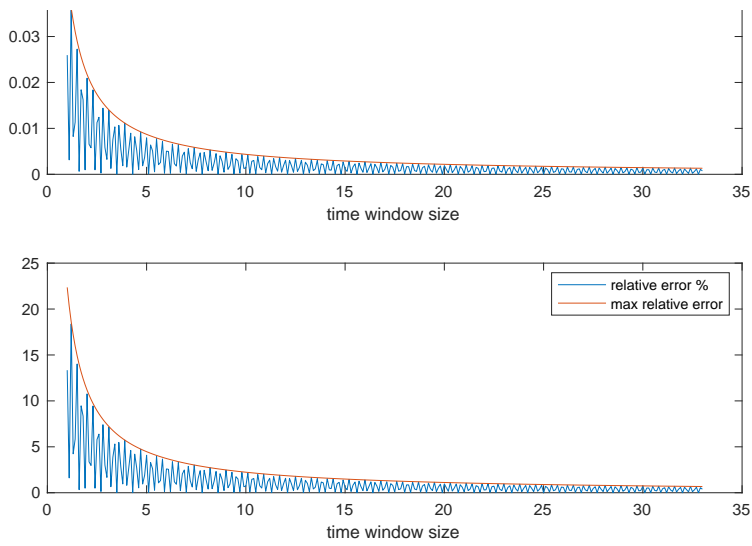
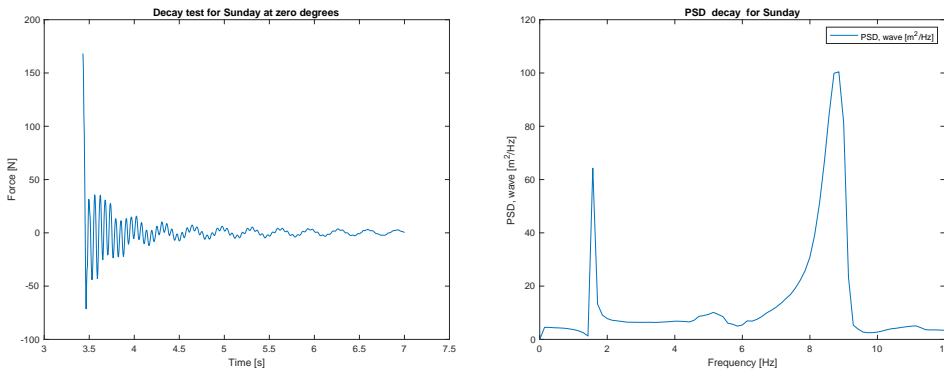


Figure 3.13: Window error when $c = 0.1945$, $a = 1.2135/\sqrt{2}$, $f = 6.281$, $t_s = 33$

3.5.2 Decay test

Decay tests are performed in water to analyze the vibrations and natural frequencies of the frame. The decay tests are done with different configurations, which will give different mass and added mass, and the natural frequency is expected to vary slightly. Also, decay tests are performed when the construction is positioned at different angles, to investigate if this changes the result. By hitting the construction with a small hammer, the vibrations are induced in the x-direction. The hit is applied on the front frame, just underneath where the load cells are connected.

The time series of the decay tests show that the damping does not follow a hyperbolic decaying as it should do, and the logarithmic decrement cannot be found. This is illustrated in Figures 3.14a and 3.15a. Further plots are in Appendix 5.6. For an angle of 0° it resulted in two large energy peaks in the PSD, seen in Figure 3.14b. The peaks are around 1 and 4 Hz on first days of the experiment and about 2 and 9 Hz on the last day, which is due to the different configurations. For angles larger than 0° the peak is given about 1 Hz, with many more smaller peaks, seen in Figure 3.15b. The reason for the varying measured frequencies could be caused by the fastening point of the frame. The fastening point for the frame to the rest of the structure is only carried by the load cells at one point and the hammer hit caused the different parts of the structure to vibrate. The natural frequencies come from both the frame and the structure. At zero degrees it results in two major frequencies peaks, while at other angles, the frame and structure have different behavior.



(a) Timeseries of decay test at 0°

(b) PSD of decay test

Figure 3.14: Test done on the last day at 0°

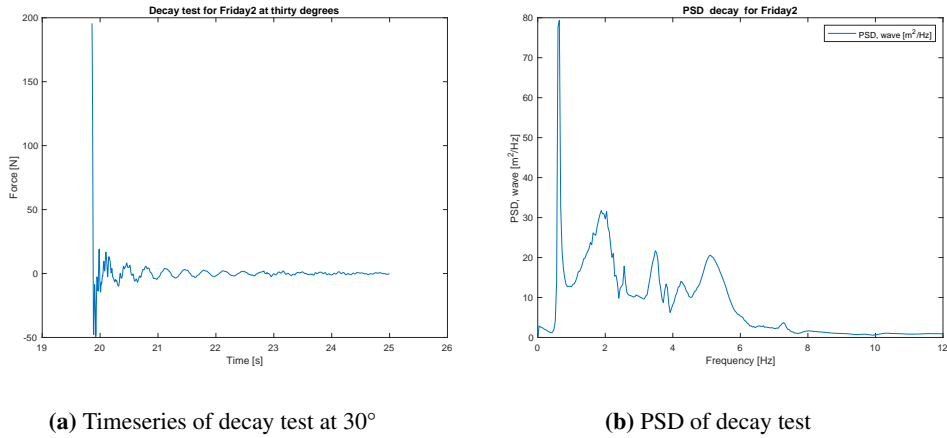


Figure 3.15: Test done at 30°

3.5.3 Forces on net section

The final values presented in the results is forces on the net section. The net section is an area of 178 mm x 178 mm, seen in Figure 3.16. The forces on the net section is calculated from the mean forces of the net panel, vertical twines, horizontal twines and the frame alone. It is assumed that the forces on the twines are evenly distributed over the length. The mean forces on the net section is be calculated according to Equation 3.6

$$\text{netforce} = \text{fullforceNET} - \text{fullforceHORIZONTAL} * \frac{322}{500} - \text{fullforceVERTICAL} * \frac{322}{500} \quad (3.6)$$

Drag and lift net forces for all angles are plotted against the run speed, U . From this, the drag and lift coefficients are found from the mean force, the projected area of the net(A), the density of the water(ρ) and current velocity(U), as Equation 3.7 and 3.8 describes

$$C_D = \frac{2F_D}{\rho A U^2 (\cos\theta^3 + 1)} \quad (3.7)$$

$$C_L = \frac{2F_L}{\rho A (U \cos\theta^2)^2 \sin\theta} \quad (3.8)$$

Here, the projected area for the net section(A) is based on the clean twine area, which is $0.015m^2$ in total. It is adjusted to account for only the net section part and number of twines. ρ is given as $1000 \frac{kg}{m^3}$. The area of a clean twine is used for calculating coefficients on both the clean and fouled net section. It could be argued that the area should include the hydroids. This is difficult to measure reliably and also includes another variable to take into account.

The drag- and lift coefficients can then be plotted against Reynolds number, which is calculated by the test speed, clean twine diameter, and kinetic viscosity.

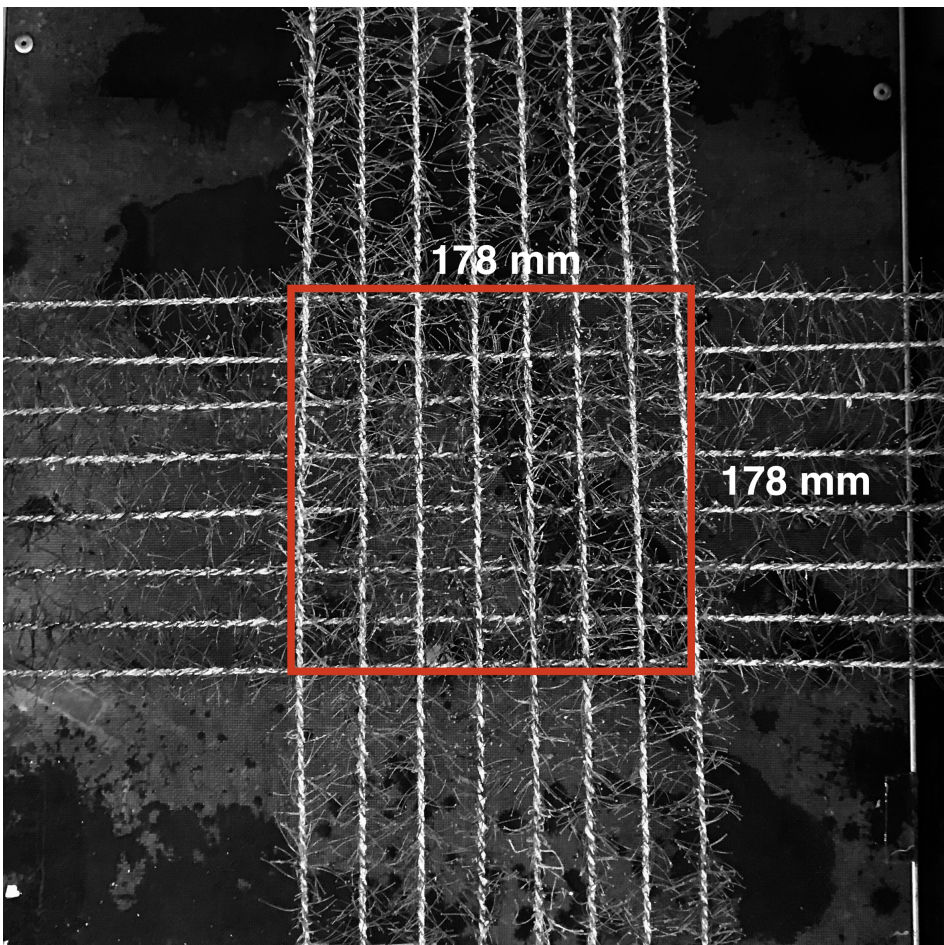


Figure 3.16: Net section

3.6 Accuracy and precision

Some tests are repeated several times to give an estimate of the precision error and uncertainty of the measurements. Any uncertainty analysis aims to give a quantitative measure of how reliable a measured or calculated value is. (Steen, 2014) Uncertainty is the statistical representation of the error. The precision limit and uncertainty are calculated using the Student's-t distribution, as will be described later. The analysis is performed on a selection of configurations. They are described in Table 3.4 and 3.5, giving the measurements for each run and the average. The Student's-t distribution is used for small samples (< 20) and is therefore suitable here.

Config- uration	Speed [m/s]	Angle [°]	Total drag [N]			Average \bar{X} [N]
			Run1	Run 2	Run 3	
8bionet	0.35	45	8.382	8.226	8.459	8.355
6fht - vert	0.05	45	0.2732	0.2633	0.2724	0.2696
6fht - vert	0.10	45	0.599	0.5894	0.6071	0.5985
6fht - vert	0.20	45	1.835	1.919	1.859	1.871
7ft - hor	0.25	0	3.567	3.491	3.456	3.489
7ft - hor	0.30	0	4.755	4.496	4.549	4.6

Table 3.4: Drag data

Config- uration	Speed [m/s]	Angle [°]	Total lift [N]			Average \bar{X} [N]
			Run1	Run 2	Run 3	
8bionet	0.35	45	0.778	0.8109	0.7902	0.7816
6fht - vert	0.05	45	0.2010	0.2179	0.2543	0.2244
6fht - vert	0.10	45	0.2615	0.2722	0.2555	0.2631
6fht - vert	0.20	45	0.3943	0.3862	0.4033	0.3946
7ft - hor	0.25	0	-0.0734	-0.03044	0.08692	-0.002308
7ft - hor	0.30	0	-0.1065	-0.01752	0.04094	-0.0277

Table 3.5: Lift data

When estimating the precision error and uncertainty in repeated tests, it is common to assume that if the experiment is repeated indefinitely times, the distribution will be Gaussian around a mean. The distribution of a confidence interval is defined as Equation 3.9,

$$Prob(X_j - t\sigma \leq \mu \leq X_j + t\sigma) = \gamma \quad (3.9)$$

where γ is the confidence interval, which is 0.95 on this occasion. It means that there is a 0.95 probability that the true value will be within the confidence interval. When, σ , the number of samples of the parent distribution, is unknown, t from Student's distribution is also unknown. The equation can be rearranged to 3.10,

$$Prob\left(-t \leq \frac{X_j - \mu}{S_x} \leq t\right) = \gamma \quad (3.10)$$

where the variable $\frac{X_j - \mu}{S_x}$ is random and follows a Student's t distribution with N-1 degrees of freedom. The standard deviation, S_x , of each test is calculated using built-in function from Matlab, based on the average value. By taking the inverse of the cumulative density function for the t-distribution, the value of t is found;

$$t = F^{-1}\left(\frac{1}{2}(1 + \gamma)\right) \quad (3.11)$$

and the result is $t = 4.3026$ for N samples = 3. The result is calculated using Excel function TINV(1-0.95; N-1). The precision limit, P_x , for a sample is then found from 3.12 and the uncertainty of a single test in the sample is given in percent as Equation 3.13.

$$P_x = tS_x \quad (3.12)$$

$$Uncertainty[\%] = \frac{P_X}{\bar{X}} * 100 \quad (3.13)$$

The standard deviation of the mean of the test in the sample is given in Equation 3.14 along with the mean precision limit and uncertainty for the mean in Equations 3.15 and 3.16. The calculation is done for the drag and lift forces in Table 3.6.

$$S_{\bar{X}} = \frac{S_X}{\sqrt{N}} \quad (3.14)$$

$$P_{\bar{X}} = tS_{\bar{X}} \quad (3.15)$$

$$Mean \ uncertainty[\%] = \frac{P_{\bar{X}}}{\bar{X}} * 100 \quad (3.16)$$

The measurements of the drag and lift forces for the repeated configurations are found in Tables 3.4 and 3.5. For the velocity of the towing carriage, the same calculations are done, and they are found in Appendix 5.7. It shows that all repetitive tests give the same value and therefore the same average. In Tables 3.6, 3.7 and 3.8, the uncertainty for each run and the mean uncertainty for all runs is listed. For drag force, the uncertainty per test is varying from as low as 6.099% to 12.79%. It is not possible to see a trend for which velocities and angles there are most uncertainty, due to shortage of repeated tests. For lift, the uncertainty is ranging from 9.813% - 16.72%. There is a clear relation between increasing velocity and decreasing uncertainty. For some configurations, a negative lift value is measured and the uncertainty cannot be measured. For velocity measurements, the uncertainty per run is extremely low, less than 1%.

Config- uration	Speed [m/s]	Angle [°]	S_x std	P_x	Uncert. [%]	Mean uncert. [%]
8bionet	0.35	45	0.1184	0.5096	6.099	3.52
6fht - vert	0.05	45	0.005482	0.02359	8.748	5.05
6fht - vert	0.10	45	0.008867	0.03815	6.375	3.68
6fht - vert	0.20	45	0.04197	0.1806	9.264	5.35
7ft - hor	0.25	0	0.05663	0.2437	6.952	4.01
7ft - hor	0.30	0	0.1367	0.5884	12.79	7.38

Table 3.6: Uncertainty drag

Config-uration	Speed [m/s]	Angle [°]	Sx STD	Px Precision	Uncert. [%]	Mean uncert.
8bionet	0.35	45	.01802	0.07754	9.813	5.67
6ft - vert	0.05	45	40.00929	0.03997	16.72	9.65
6ft - vert	0.10	45	0.008449	0.03635	13.82	7.98
6ft - vert	0.20	45	0.009995	0.043	10.27	5.93
7ft - hor	0.25	0	0.0817	0.3515	-1.523e+04	-8.79e+03
7ft - hor	0.30	0	0.07426	0.3195	-1153	-666

Table 3.7: Uncertainty lift

Config-uration	Speed [m/s]	Angle [°]	Sx STD	Px Precision	Uncertainty [%]	Mean uncert.
8bionet	0.35	45	2.18e-05	9.38e-05	0.0262	0.0151
6ft - vert	0.05	45	4.41e-06	1.898e-05	0.03709	0.0214
6ft - vert	0.10	45	1.11e-05	4.79e-05	0.0467	0.027
6ft - vert	0.20	45	2.69e-05	0.00011	0.0565	0.0326
7ft - hor	0.25	0	2.63e-05	0.00011	0.0442	0.0256
7ft - hor	0.30	0	3e-05	0.00012	0.0420	0.0243

Table 3.8: Uncertainty velocity

The bias error is not revealed by the repetition of the experiment, it is a systematic error. For an experiment like this, it is hard to estimate the bias error since it is in the system and the system has not been tested for repetitively. That would mean building an identical model and testing it in another facility. The bias error can be estimated by a "qualified guess". The most possible bias error is the calibration of the load cells. If the calibration factor is wrong, all force measurements will also be wrong. The calibration is carried out carefully and tested twice with the same result. The calibration factor is not tested after the experiment, which would be another verification. Also, if the measurements on the net section are scaled and transferred to a real net scenario, the modelling accuracy could be a modelling accuracy is an error source. Measuring the stiffness of the hydroids is impractical and the human error is large. The difference in density between artificial hydroids and real will also be a significant error for real net applications.

Results and Discussion

4.1 Mean drag and lift forces on net section

In this section, the measurements of the forces on the net section is given. Drag and lift on both clean and hydroid fouled net panels will be presented. The figures display forces acting on the net section as a function of velocity. Measurements on clean net is described by the green lines in the figures and the legend explains forces on fouled net section, with numbers specifying angle of attack. Drag and lift forces measured for the lowest speed gives negative value for some solidities and angles. Since measurements on the net section is dependent on results from frame, frame with vertical twines, frame with horizontal twines and frame with net panel, there are many uncertainties to account for. In the event that one or more of the measurements is taken with a large error, it influences the final value. The uncertainty of drag measurements varies from 6 - 12%, while lift reaches a maximum of 16% uncertainty. It is plausible that the vertical measurements are recorded too high and/or panels too low, which gives unnatural result. Also, the zeroing of load cells can have a large influence on small forces, even when it is measured at the third decimal point. Especially for low velocity measurements, where the some forces are in fact measured at second decimal point. With this this in mind, the negative values are disregarded. In the time series it is noticed that the force measured on the frame in low speeds, gives negative value. That proposes a force acting in the same way as the towing direction. The flow pattern around cylinders does not suggest this is possible and for this reason, all measurements at 0.05 m/s is removed when coefficients are investigated.

The drag and lift on the net section of 8x8 twines is represented over speed in Figure 4.1. By comparing the force on the fouled- and cleaned twines, it is clear that the presence of hydroids on the twines increases the drag force considerable. The added projected area of artificial hydroids is the reason for this. The drag measurements is increasing as expected along the increasing speed. Maximum drag on fouled net section is measured with the flow orthogonal to the flow and lowest at 45°. For clean twines, drag is as expected, much lower. Lift for the fouled net section shows measurements around 0 N for

all angles except 45° , which reaches a maximum of 0.7 N. Measurements on net section with cleaned twines are also circulating around 0 N. Some measurements are negative and some are slightly increasing with speed. The small forces are more difficult to distinguish between, especially since the uncertainty is large.

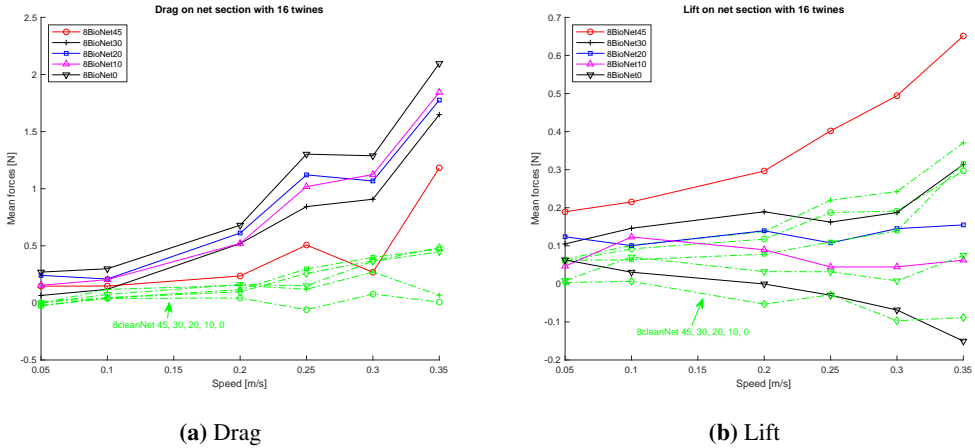
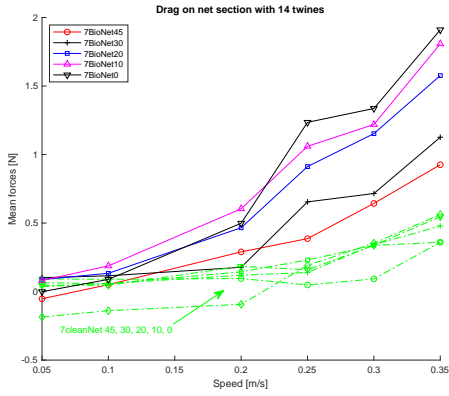


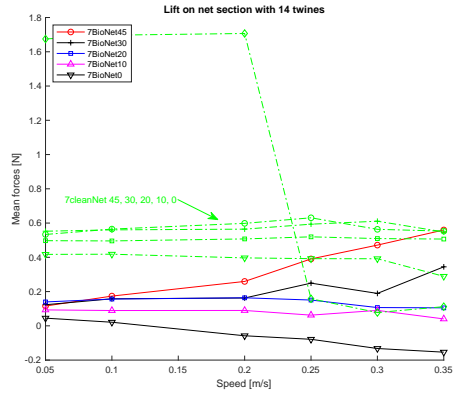
Figure 4.1: Mean drag and lift on fouled and clean section of 16 twines

Drag and lift measurements on 7×7 net section is represented in Figure 4.2. The results show the same trend as before; the hydroids amplify the drag force substantially compared to clean nets. The maximum measurement of drag force is for orthogonal incoming flow and minimum is when θ is 45° . The total drag force for fouled twines is slightly lower than for 8×8 net. For the clean net, the max drag force is slightly larger than 8×8 . Lift on fouled net section has absolute largest value when flow is incoming at 45° . For clean net, the measurements are stabilizing around 0.5 N. The values at 1.6 N for clean net is due to error in the load cell and is fixed by zeroing before 0.25 m/s. Otherwise, the lift force on clean nets is mostly higher than for fouled, which is unexpected due to the added area of the hydroids. Again, it can be due to uncertainty.

The result of forces acting on a 6×6 twines in net section is shown in Figure 4.3. It is still clear that hydroids significantly increase drag force on the net section, compared to clean twines. Maximum drag is at incoming current when angle of attack is 0° or 10° . The minimum force is clearly at 45° . Drag force on clean net is maintained around 0.1N. For lift, an angle of attack at 45° gives a huge difference for net with biofouling, while for clean net the force is not as dependent on angle of attack.

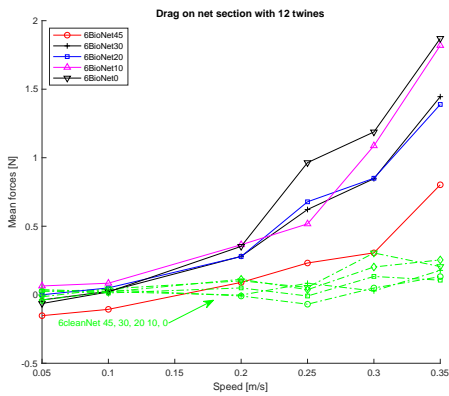


(a) Drag

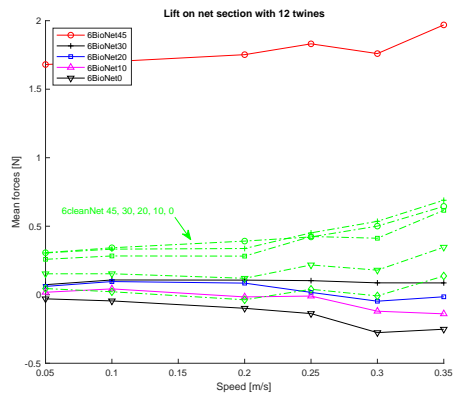


(b) Lift

Figure 4.2: Mean drag and lift on fouled and clean net section of 14 twines



(a) Drag



(b) Lift

Figure 4.3: Mean drag and lift on fouled and clean net section of 12 twines

4.2 Drag and lift coefficients

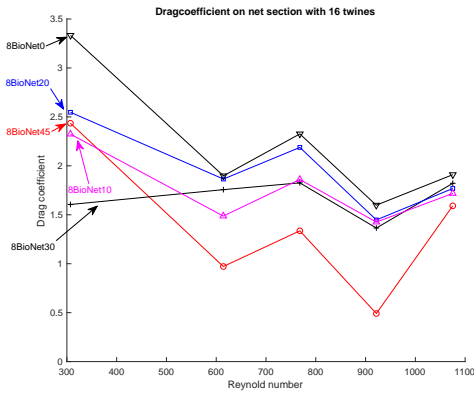
It is very convenient to investigate dimensionless drag- and lift coefficients C_D and C_L and Re , to understand the force measurements further. The coefficients are separated in figures by solidity and all angles of attack are included.

For drag coefficients in Figures 4.4a, 4.4c and 4.4e it is clear that for a flow incoming at 45° , the coefficient is lowest. It becomes more evident over increasing Re , and especially for 8x8 net section. The highest coefficient is for $\theta = 0^\circ$, but for angles in between, the measurements are fluctuating. For most net configurations and angles, there is a noticeable incline in drag forces at 750 - 850 Re . The incline is within the estimated maximum uncertainty of approximately 12%. Nevertheless, the incline is evident in all measurements, and therefore it does not appear to be an error. The incline is not present in the measurements of clean net sections, which can be studied in the Appendix 5.8. It seems to be a feature due to the hydroids on the twine, but it is difficult to give a conclusive reason without more research.

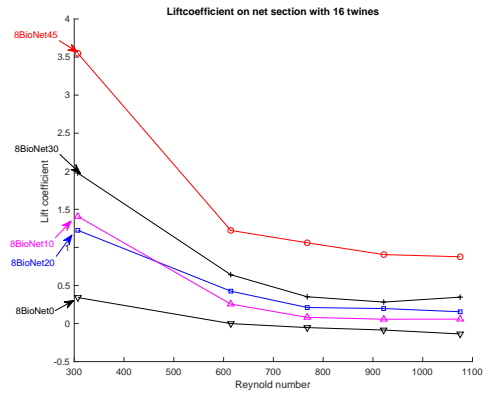
The drag coefficient is expected to decrease over Re , due to the deformation of the hydroids with increasing current exposure. In research by Lader et al. (2015), it was evident that drag coefficient on a single twine with hydroid fouling, decreases at Re 1000 - 4000. This study presents results which are not. Regarding dependency on Re , there is a clear difference between single twines and net panels with biofouling.

For lift coefficients in Figures 4.4b, 4.4d and 4.4f, it is very clear that a flow incoming at 45° gives the largest lift coefficient, for all solidities. The angle dependency is distinct and coefficients are decreasing with angle, giving lowest result when θ is 0° . All the coefficients are largest at low Re and reduces. Lift coefficients also show dependency of Re for low values, but at 650 Re it stabilizes.

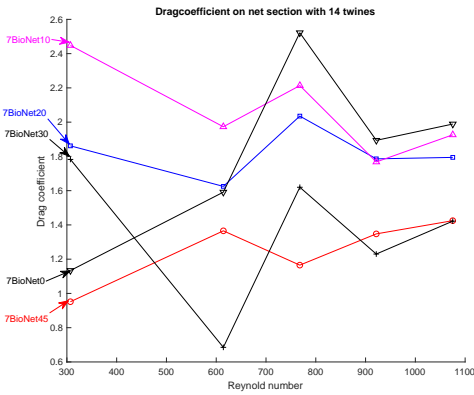
4.2 Drag and lift coefficients



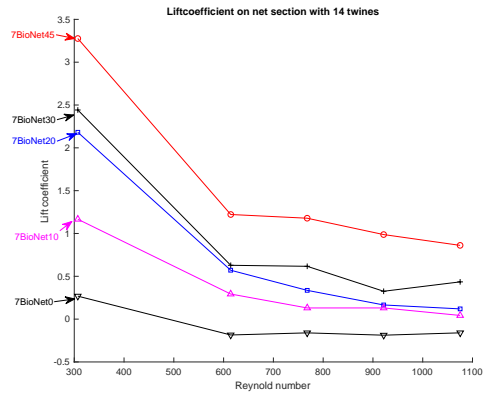
(a) Drag coefficient 8x8



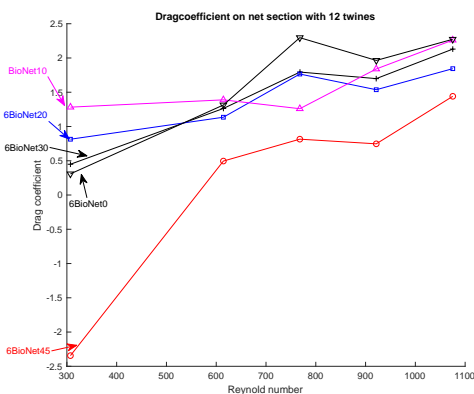
(b) Lift coefficient 8x8



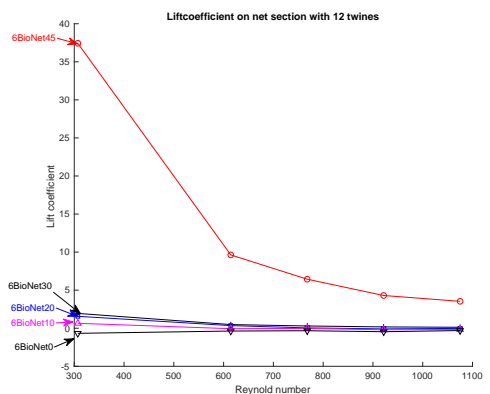
(c) Drag coefficient 7x7



(d) Lift coefficient 7x7



(e) Drag coefficient 6x6



(f) Lift coefficient 6x6

Figure 4.4: Drag and lift coefficients on fouled net sections

4.3 Comparison to Lader

The experimental data on single twines with artificial hydroids from Lader et al. (2015), is plotted for comparison to the experimental data obtained. The drag force on a single fouled twine produced a quadratic and linear term curve fit, and C_D is found from this. The comparison is for the same density and length of hydroids, with the same diameter of the twines. It is seen in Figure 4.5. Drag coefficient on net sections are clearly larger than for a single twine. A possible explanation for the difference in forces lies in the stiffness of the multifilament fishing line. The stiffness of the hydroid stem is not measured for this thesis, nor in the study by Lader et al. (2015). They hydroid deformation is described by Lader et al. (2015), is increasing with current velocity. Thus, slow current should not give large difference in the drag forces, as the deflection is small. Therefore, a more likely reason for the difference is the many crosses included in the net section compared to a single twine. Knots in a net are known to experience higher forces than the cylinders. Scaling drag force obtained from a cylinder will give unrealistic results since viscous interaction effects between cylinders/twine and spheres/knots are not considered (Fredheim, 2005). Figure 4.5 gives confidence in the reliability of the experimental data.

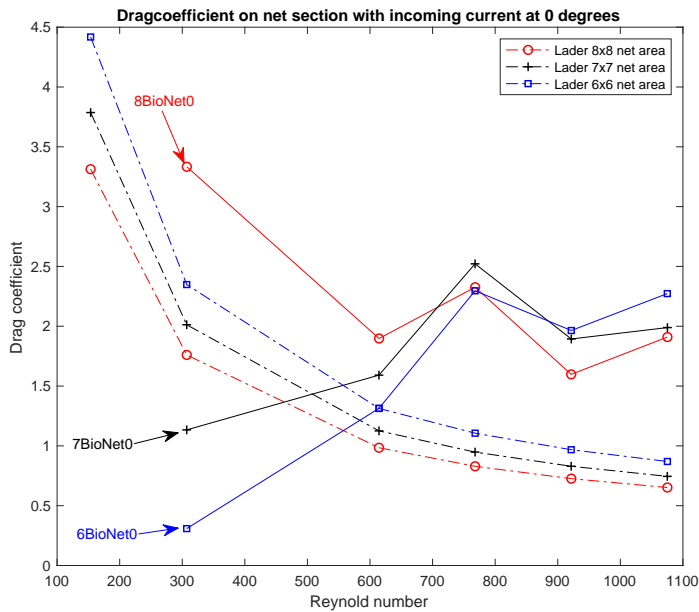


Figure 4.5: Experimental data of net section and curve fit of single twine from Lader et al. (2015)

4.4 Comparison to Løland

A comparison of coefficients from experimental results and calculated coefficients on nets is done with the estimated relationship by Løland (1991) (explained in Section 2.3). The estimated drag- and lift coefficients are dependent on solidity and angle of attack, and does not consider Reynolds number. The reasoning for this lies in the validity of the formula, which is for Re between 1400 and 1800. From Hoerner (1965) estimation of the drag coefficient on smooth cylinders and sphere, the coefficient is constant and equal to one over this area of Re . It is assumed this is correct for clean net panels also, and therefore the equation has no dependency on Reynolds number. Re tested for in this experiment is between 307 and 1075. As mentioned, the drag results are characterized as relatively independent of Re , while lift is uncertain. The coefficients are plotted against the estimation by Løland (1991) to see clearly if the measurements from the experiments are dependent on Re or not. Also, since the formula is developed from experiments on clean net panels, the net section with biofouling should obtain larger coefficients. Both the experimental results and the estimation of clean nets by Løland (1991) are included in every figure, sorted by solidity. Figures for all angles are created and 10° and 45° are chosen for illustration. The rest of the comparisons are available in Appendix 5.9.

4.4.1 Clean twines

Drag

First, the experimental drag coefficients on clean net section is compared to the estimation of coefficients. The correlation will give a validation of the results as they are examined further. Figure 4.6 shows that the measurements are very close to the estimated value, while 4.7 shows both negative and very high values. The negative values are disregarded, and so is the high anomaly point. Since most of the measurements are close to the estimated value by Løland (1991), further analysis is made by looking into dependency on angle of attack and solidity for clean twines.

An average of drag coefficient over Re is calculated for every solidity and corresponding angle. In Figure 4.8 both the estimation and data measurements of C_D is plotted versus angle of attack. The best fit is the polynomial trend line, chosen by the coefficient of determination (R^2). All the equations for the trend lines are found in Appendix 5.10. The estimation by Løland (1991) is plotted as the green lines. Measurements for from towing tests with clean net panel is decreasing with angle of attack, which is similar to what is expected. For a solidity of 0.19, the data points are lower and for a solidity of 0.237 it somewhat large, but both are considered reasonable. Figure 4.9, illustrates the same data sets, with a different representation. Drag coefficient is plotted against solidity from 0.19 to 0.28. Linear trend lines are the best fit. The estimation of coefficients is again represented as the green lines. It is difficult to see the trend lines for all angles, however, the intention is only to evaluate if the experimental results are accurate. Regarding both representations of results, the comparison to the estimation of drag force on clean net panels is evaluated fair and the setup gives representative measurements.

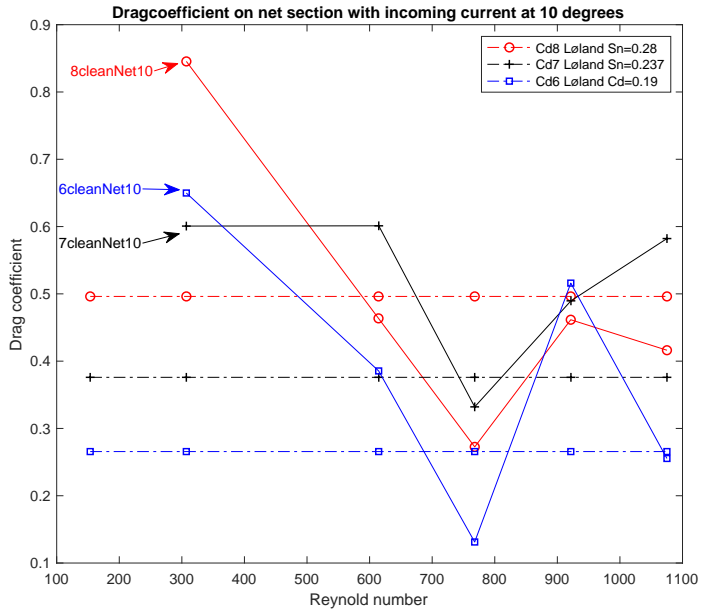


Figure 4.6: Drag coefficient at 10° on clean nets

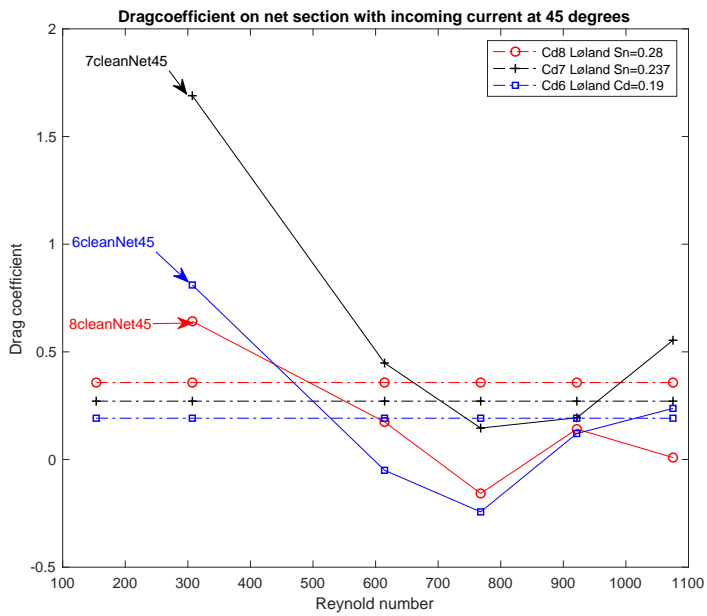


Figure 4.7: Drag coefficient at 45° on clean nets

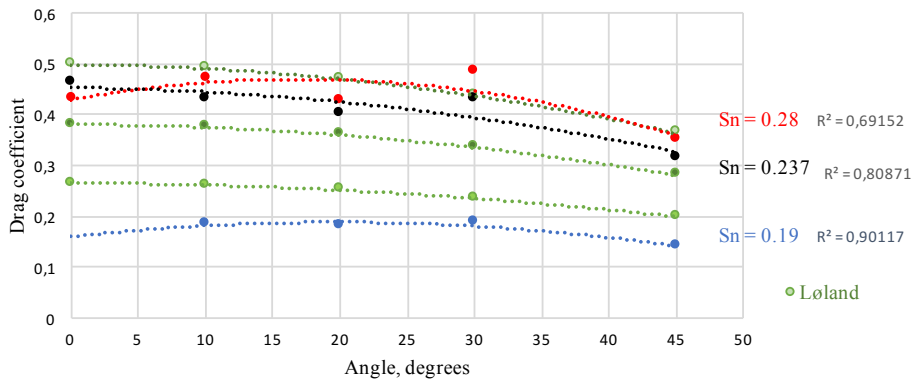


Figure 4.8: Second degree polynomial trend line fitting drag measurements on clean net, plotted versus angle of attack, and Løland's estimation

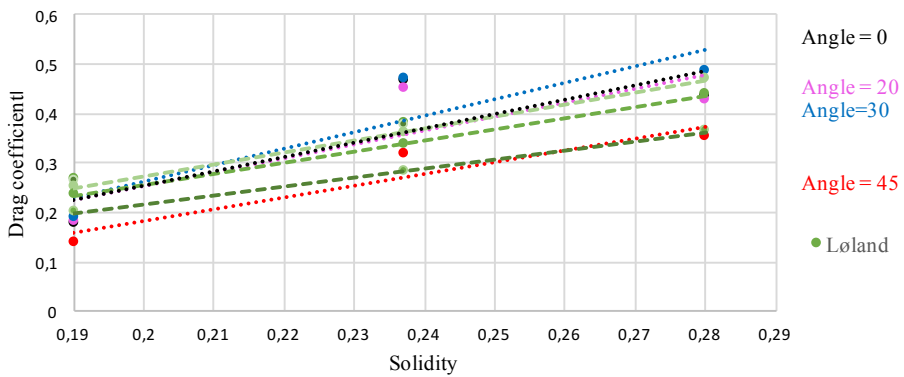


Figure 4.9: Linear trend line fitting drag measurements on clean net, plotted versus solidity and Løland's estimation

Lift

Lift coefficient in Figures 4.10 and 4.11 show a strong dependency with Re and the first measurements are specifically much higher than the estimated values. The measurements does not necessarily have to be wrong, but for low Re , the estimation by Løland (1991) cannot be expected to be correct for lift coefficients. The measurements after $Re = 600$, can still be studied further with comparison to the estimation. Figure 4.12 shows the acceptable values for each angle of attack, sorted by solidity. Values at 0° is assumed zero and the measurements at an angle of 10° are overlooked due to negative measurements. The clean net estimation of coefficients is plotted as the green lines. The Figure illustrates how experimental data on the clean net deviates from the expected. Especially the results for $Sn = 0.19$ and 0.237 is far from the estimated. The uncertainty of the lift force is at a maximum of 16%, which could explain some of the deviation, but the coefficients would still be large. Otherwise, the load cells are a potential cause for the high forces. The load cells expect larger forces and the precision is not as good for low forces.

Figure 4.13 shows the same data set, but lift coefficients are plotted against solidity. While the estimated coefficients by Løland (1991) gives a slight increase in coefficients with solidity, the experimental results for clean net does not. The experimental lift coefficients are decreasing with solidity. It can also be questioned if the calibration is done correctly, even though it is executed twice.

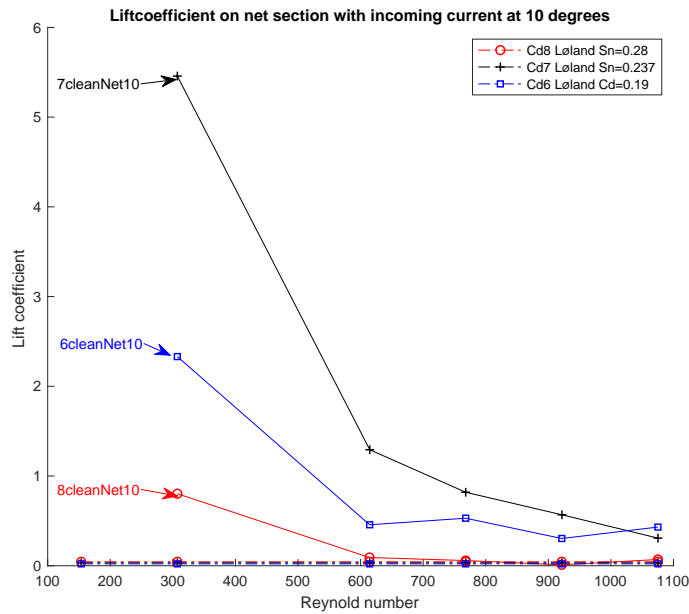


Figure 4.10: Lift coefficient at 10° , on clean nets

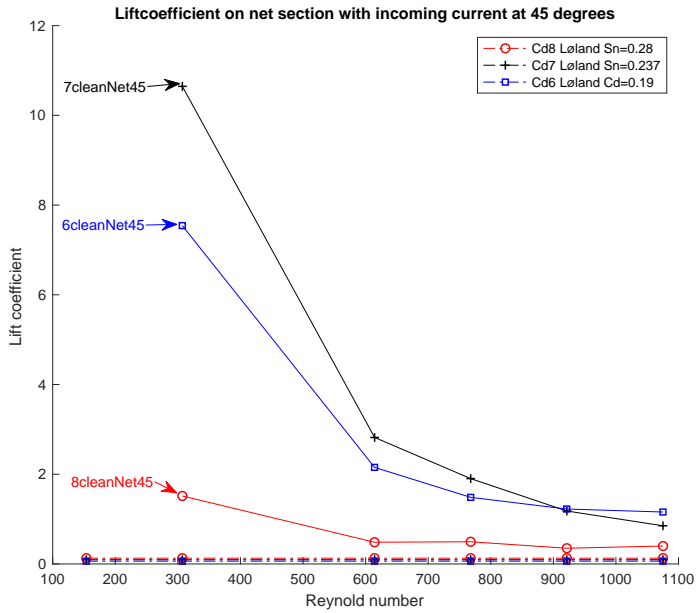


Figure 4.11: Lift coefficient at 45°, on clean nets

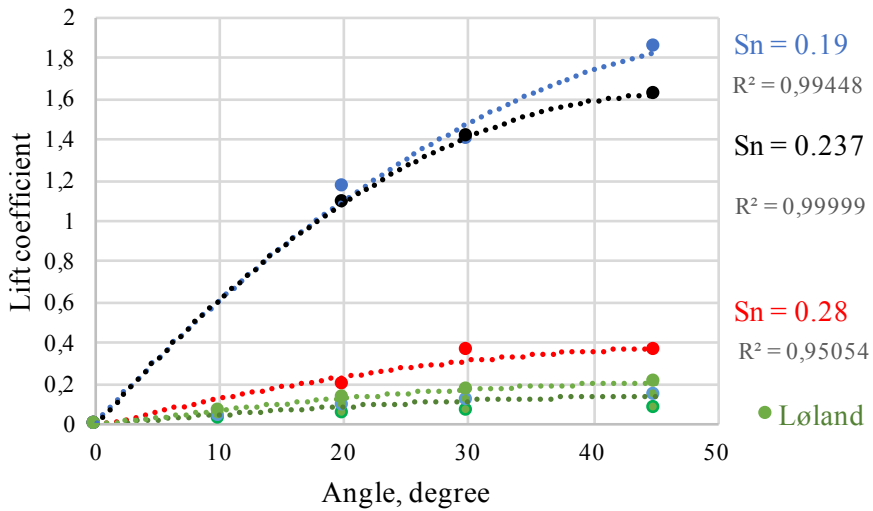


Figure 4.12: Second degree polynomial trend line fitting drag measurements on clean net, plotted versus angle of attack, and Løland's estimation

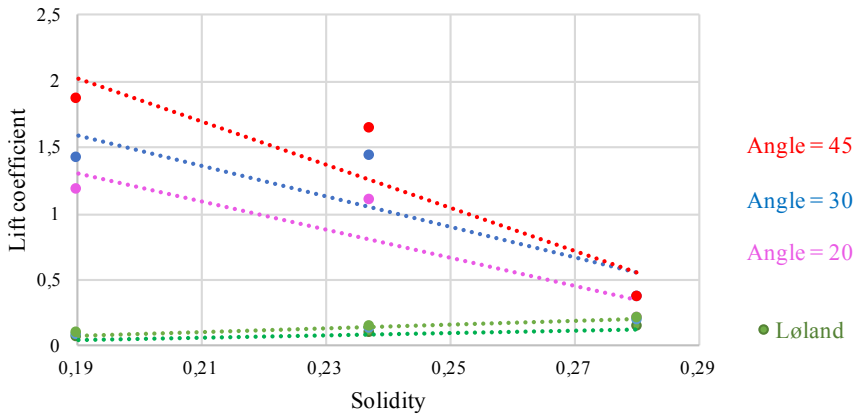


Figure 4.13: Linear trend line fitting lift measurements on clean net, plotted versus solidity and Løland's estimation

4.4.2 Twines with biofouling

Drag

Drag coefficients on models with artificial hydroids are also compared to the estimated coefficients by Løland (1991). First of all, the goal is to evaluate the dependence on Reynolds number. Secondly, evaluate the importance of solidity and angle of attack for fouled nets. From the first examination of Figures 4.14 and 4.15, it is clear that the presence of hydroids gives a larger drag coefficient compared to the formula for clean nets. The projected area of the artificial hydroids are not accounted for in calculating coefficients and naturally this gives a larger coefficient. Over this range of Re the incline at 700 - 800 is not very noticeable with flow incoming at either 10° or 45° . The coefficients of solidity 0,19 (blue line) is increasing and is the largest point for the last measurements, but with this representation of results, is not certain which solidity gives the largest average coefficients.

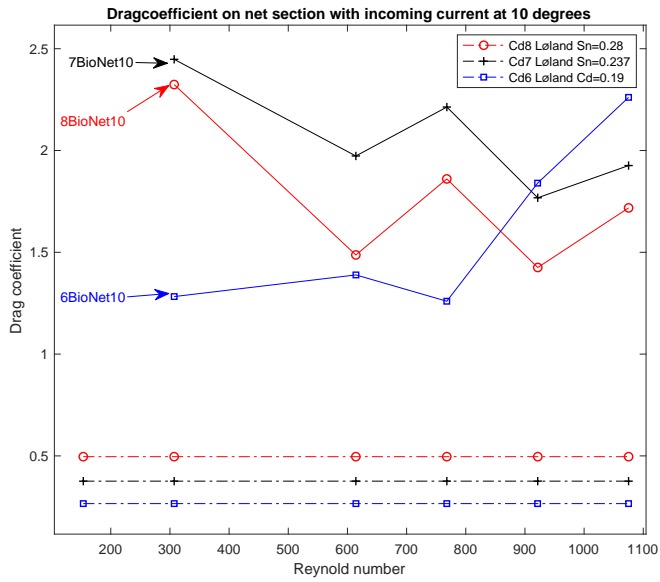


Figure 4.14: Drag coefficients at 10°, on fouled nets

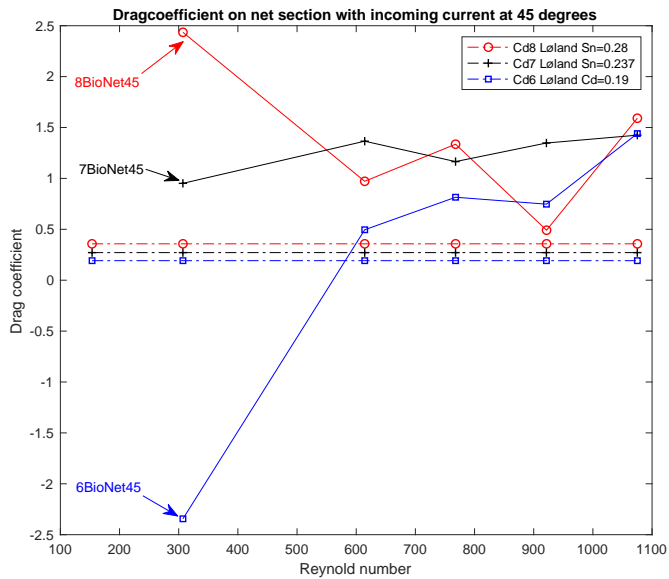


Figure 4.15: Drag coefficients at 45°, on fouled nets

The data points over Re fits a linear function best, and are therefore not dependent on Reynolds number. An average of C_D for all angles and solidities is calculated and evaluated by its relevance to solidity and angle of attack. The data points for C_D over angle, fits a second degree polynomial trend line, seen in Figure 4.16. The coefficient of determination (R^2) fits the data point at 0.95, 0.95 and 0.99. Four data points from the data set are used to create the best fit. The coefficients are decreasing with larger angle of attack, as expected. The curves of experimental results and the estimation of Løland (1991) follows the description of Equation 4.1. As mentioned, all the equations for the trend lines are found in Appendix 5.10. The curving is described by A , which is descending mostly for solidity of 0.237. B describes the linear reliance, which is most present for a solidity of 0.28. This could be random, as the uncertainty of the measurements can slightly change the curving or linear reliance. It is still very evident that the angle dependency for hydroid fouled nets is greater than for clean nets. The area of the biofouling is the most obvious reason, because the added area of the hydroids is not included in the calculation of the coefficient. As known from the calculation, velocity is irrelevant and the angle of attack is the same for clean and fouled nets, ergo, the projected area is the difference. The large decrease in the forces is due to the deformation of hydroids on net panels at different angles of attack. As the angle of attack in increasing, so is the deformation.

Table 4.1 provides an over view of the percentage decrease in coefficient over angle. The decrease in forces is about twice as great for fouled nets. It appears to be decreasing with larger solidity, but as mentioned, slight changes in the steepness can be due to the uncertainty.

$$- A * (angle)^2 - B * (angle) + C \quad (4.1)$$

Drag coefficients are increasing with solidity, at a linear phase. This is illustrated in Figure 4.17. The trend lines of the experimental results and Løland (1991), follow the Equation of 4.2. The slope, D , is twice as steep for hydroid fouled nets than clean. Again, the area of fouling is important. With larger solidity, more biofouling is introduced and the steepness is larger than for clean nets. The slope should be increasing at same value for all angles. There are deviations in the measurements, probably caused by uncertainty in the measurement of forces. Nonetheless, solidity and angle of attack is more important for hydroid fouled nets.

$$D * Sn + E \quad (4.2)$$

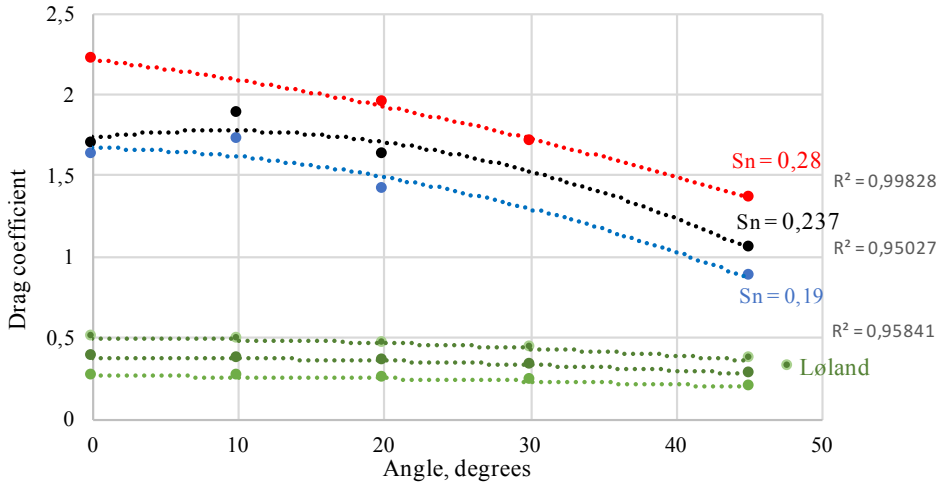


Figure 4.16: Second degree polynomial trend line fitting drag measurements on fouled net, plotted versus angle of attack

Type net/ solidity	0.19	0.237	0.28
Clean net	25%	26%	27%
Hydroid fouled net	53%	45%	40%

Table 4.1: Percentage decrease of the drag forces with over angle 0°- 45°

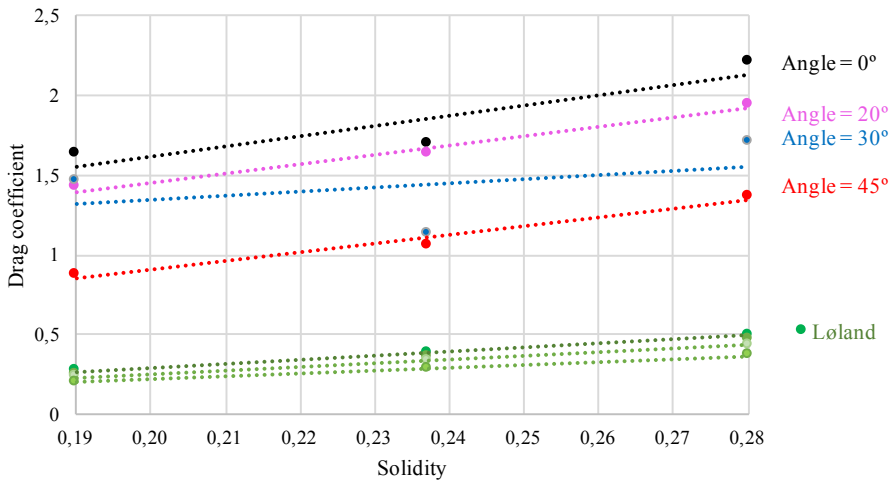


Figure 4.17: Linear trend line fitting drag coefficients on fouled net, plotted versus over solidity

Lift

In Figures 4.18 and 4.19, the presence of hydroids is also distinct, and gives a larger drag coefficient compared to the estimation for clean nets. *6BioNet10* is removed from the graph, as almost all measurements are negative. When presenting the results at a fixed angle and given solidities, the Reynolds number dependency is clearer. The extreme values for lift at 45° for *6BioNet45* deviates from the other results and is unlikely. After $Re = 600$ the lift coefficients are stabilizing and not as dependent on Reynolds number. An average C_L is calculated for Re between 614 - 1075 and described by their relevance to solidity and angle of attack. A second degree polynomial trend line is fitted to the results shown in Figure 4.20, with R^2 equal to 0.99. Solidity of 0.19 has negative results for 0°, 10° and 20°, and is excluded from the comparison. The lift coefficient is increasing with angle of attack. The curve for experimental lift data has a positive term for the curving, while the estimated lift data does not. If the measurement at 45° is reduced with the possible uncertainty of 16% and the measurement at 20° is increased by the same amount, the curving become negative for $Sn = 0.237$ and $+0.0002$ for $Sn = 0.28$. It is unexpected that the largest solidity does not produce the largest lift coefficient. However, this is also the fact for experimental data of clean nets. It could be a result of the load cells.

For lift coefficient and solidity, a linear trend line is estimated by Løland (1991). In Figure 4.21, a second degree polynomial curve fits the measurements best. As mentioned, lift measured from clean nets did not fit the estimated value from Løland (1991) and it is questioned if the setup for lift forces is unreliable.

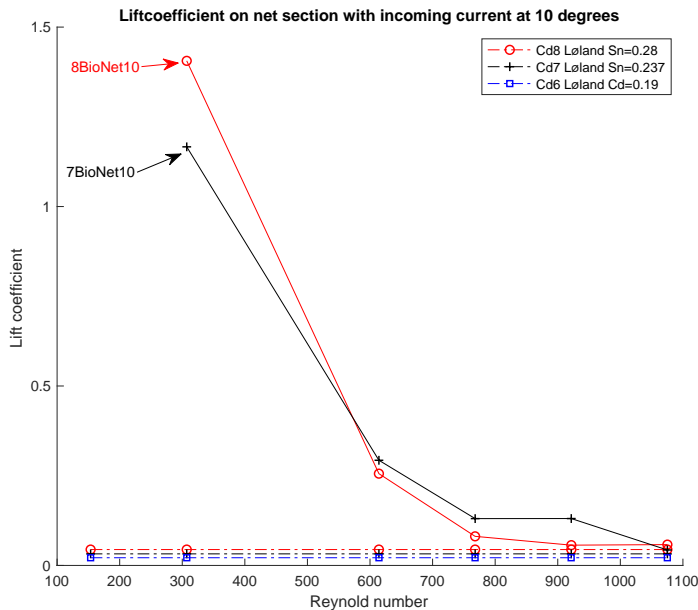


Figure 4.18: Lift coefficients at 10°, on fouled nets

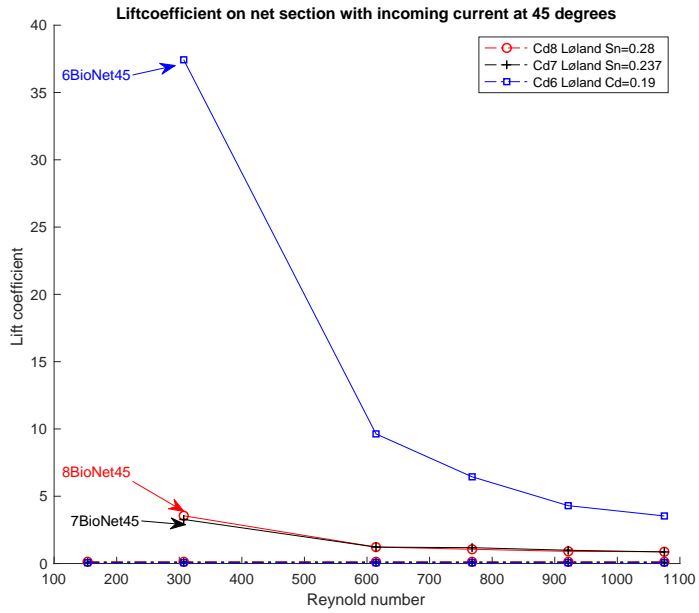


Figure 4.19: Lift coefficients at 45°, on fouled nets

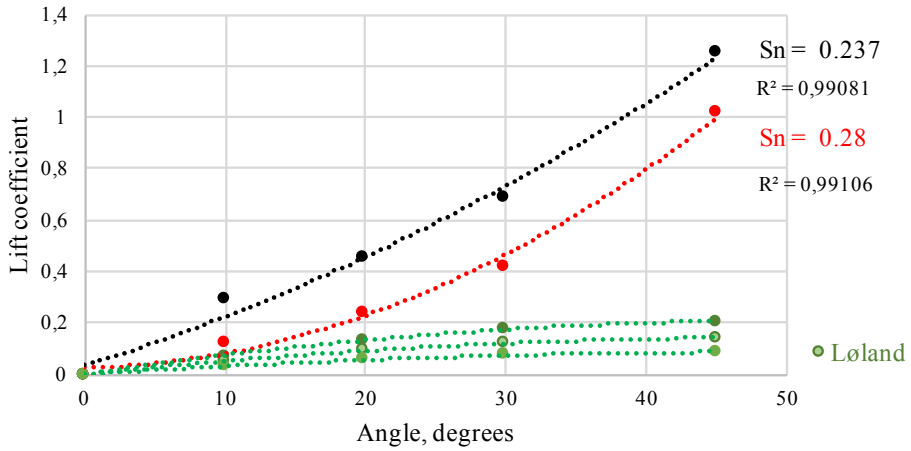


Figure 4.20: Second degree polynomial trend line fitting lift coefficients on fouled net, plotted versus angle of attack

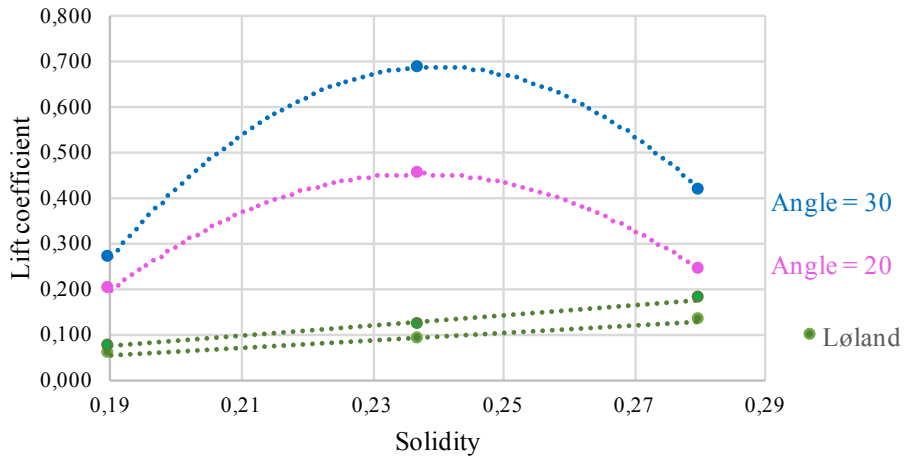


Figure 4.21: Second degree polynomial trend line fitting lift coefficients on fouled net, plotted versus solidity. The clean net estimation follows a linear trend line

4.5 Errors

Possible error sources are listed in order to point at elements which might explain the negative forces from measurements and the large uncertainty in the Student-t calculation. The force measurements are dependant on a constant towing velocity, a steady current flow, the stiffness of the fastened twines, stiffness of the artificial hydroids, correct solidity and angle, and the accuracy of the load cells. The total force is dependent on measurements from several configurations and the calculation of mean force in post-processing.

- The repeated tests of the towing carriage speed gives little uncertainty. It is recorded at below 1% for all speeds, which is incredible low. The current velocity is therefore very reliable at all speeds.
- However, the flow along the water depth can fluctuate from the measured towing velocity. The frame and twines reach minimum 10 cm below the water line and maximum 60 cm. The current is assumed to be uniform with increasing depth, and the forces are distributed evenly on the whole twine. The tank has not recorded issues with fluctuations before and it is not expected to have large influence on the end result.
- The twines are fastened in the frame by clamping two parts of the frame and tightening with screws. This occurs every time the twines change configuration. It is important that the twines remain rigid during the towing, to avoid flexibility of the twines, which reduces forces. The twines are tightened to the authors acceptance but no guarantee of pretension can be given. This can lead to bending in some twines, an error which is unknown.
- Moreover, the placement of the twines with regards to half mesh, is done manually. For increased reliability, the distance of the half mesh is reviewed several times. Since the solidity of the net is an important factor for the total force, it could been done with more precise methods.
- The stiffness of the hydroids affects the deformation and consequently the measured force. The stiffness is not qualitatively assessed in the experiment, only a visual comparison to hydroid used by Lader et al. (2015) is done. At low Reynolds numbers, the difference in deformation should not be significant and it is a minor error.
- Another important factor for the total force measurements is the angle of attack. The frame is arranged to correct angle by manually turning it and checking according to a protractor. If the protractor is slightly inaccurately mounted, it will be a bias error since all measurements are dependant on it.
- In addition, the load cells have to be calibrated correctly and chosen to fit the experiment. In this experiment the load cells are calibrated twice and zeroed every time the structure is pulled out of water. It can be argued that the load cells of 18 kg have too large range when the expected forces are much lower. Especially for lift forces. However, it is the only load cells available at NTNU.

- Furthermore, the total force on the net section is dependant of the calculation of forces from the frame alone, frame with horizontal twines, frame with vertical twines and frame with twines in net panel. The accuracy of the total force on net section is affected by all of these measurements and thus the total uncertainty is unknown.
- The post-processing and calculation of mean force impact the total force used in further analysis. The total force is the mean force from the steady phase during towing. The twitching in the towing carriage, fluctuations in the flow and vibrations in the structure causes the measured forces to oscillate. The eigenfrequency of the structure are found from PSD plots and show multiple peaks due to intertwining of frequencies from various parts of the structure. This is one reason for the oscillation. The mean is calculated from of integer points of a time window with uncertainty below 1%, which gives high confidence in the mean force.

The uncertainty calculated from the repeated tests are somewhat high for lift, while acceptable for drag and extremely low for the velocity. The uncertainty is calculated based on only N samples = 3. When the number of samples are below 10, there is a rapid decrease in the precision limit with increasing samples. Thus, if more repeated tests are done, the precision limit and uncertainty will decrease. Also, the replication level of the repeated tests is not very diverse. The uncertainty of the forces varies with velocity, angle and configuration. The uncertainty analysis indicates velocity as a triggering factor for the lift force, but not trend is found for the drag force.

Conclusions

5.1 Experimental testing

The aim of this master thesis is to compare experimental drag- and lift coefficients from net panels with biofouling, with established methods for calculating coefficients on net panels. The primary objective is to describe a method for designing and executing a range of experiments related to the solidity and angle of attack on a rigid net section with fouling. This is completed by creating clean- and fouled twine models and building a structure for towing the net panels. Configurations with Sn of 0.28, 0.237 and 0.19 gives data to evaluate the trend of solidity, while an angle of attack at 0° , 10° , 20° , 30° and 45° provides enough values to evaluate the dependency of the angle. The length of the artificial hydroids is 16 mm, which corresponds to about 70 days of growth. The experiment is tested for Reynolds number 170 - 1100, but valid for Re 300-1100 for drag and Re 600 - 1100 for lift. The runs done with a velocity of 0.05 m/s are excluded due to negative measurements of drag and lift force on the frame, and the lift measurements at 0.1 m/s are also excluded for the same reason. The uncertainty of the experiment is below 1% for the towing carriage, between 6 - 12% for the drag force and 9 - 16 % for the lift force. The uncertainty is based on repeated tests at different velocities, angles of attack and configurations. Comparison of coefficients on the clean net section with the estimated of coefficients from Løland (1991), are evaluated as fair and the setup gives representative measurements. A comparison to similar experimental data from Lader et al. (2015) also gives confidence in the reliability of the drag results.

The secondary objective is to assess the difference in drag- and lift forces on clean nets in comparison to hydroid fouled nets. It is clear that the presence of the hydroids amplifies the forces considerably. This is most evident for the drag force. The drag force measured at an angle of attack at 45° distinctly gives the lowest value for all solidities and the drag force at 0° is largest. The results match the expected trend with respect to the variance in the projected area with angle. For a clean net, the importance of angle is not as evident for the drag the force. Some measurements are also negative and not considered further.

The lift force for a fouled net is increasing steadily with speed and it is obvious that angle dependency matters. At 45° , the lift force for nets with biofouling is especially large.

The last objective is to evaluate if the coefficient from nets with biofouling is dependant on Reynolds number, solidity and angle of attack. Some drag coefficients plotted versus Re , show an incline in forces at 700 - 800 Re . A linear trend line is still the best option for the data set and they are independent of Reynolds number, which is not expected for clean and hydroid fouled single cylinders (Hoerner, 1965) (Lader et al., 2015). This study concludes that there is a clear difference between drag force on a single twine with fouling and net with fouling, regarding Re dependency. An average of C_D for all angles of attack and solidities are calculated and evaluated by its relevance to both variables. Drag coefficients are decreasing with the angle of attack, fitting a second degree polynomial trend line with negative curving. The angle dependency for fouled nets is greater than for clean, and in percentage, it gives twice the decrease of clean nets. It appears that the deformation of the hydroid on net panels is greater for larger angles of attack. The increase in C_D for increasing solidity is linear. The steepness is greater for hydroid fouled nets than clean. The reason for this is the extra projected area from the hydroids which is increasing with solidity. For lift coefficients, it is not clear if the data is acceptable. First of all, the uncertainty of lift measurements is large and the load cells are not well-suited for such low forces. A comparison to Løland (1991) is made for clean twines at Re above 600, but it did not follow the expected trends. Experimental lift coefficients of a net panel with biofouling, fit a polynomial curve with positive curving when plotted against the angle of attack. With regards to solidity, the lift coefficients are not increasing linearly but fits a polynomial curve with negative curving. When the uncertainty is included in the results, the curve shifts coefficient but the main shape remains. It is unknown if the results are due to a bias error for lift measurements or a phenomenon of the hydroids.

In summation, it is not possible to simply add a coefficient to the formula by Løland (1991), or increase the twine diameter. The update needed to assure technical approval in NS9415 for fouled nets, is a formula for drag coefficients based on solidity and angle of attack. Net panels with biofouling are independent of Re , and due to this, the coefficient by Hoerner (1965) cannot be used. Neither can the formula by Løland (1991), since nets with biofouling are more dependant on the angle of attack and solidity.

5.2 Recommendations for further work

The aim of further work on this topic should be to complete a functional relationship for the drag and lift forces on nets with biofouling, with less limitations than mentioned here. This study has opened a discussion about the need for a reliable calculation of drag forces on aquaculture nets with biofouling. The required research to establish a requirement for NS9415, is to do more testing with higher current velocity, measure the stiffness of the hydroid stem and establish an empirical formula of C_D and C_L .

Testing of net panels with fouling at higher current velocity, is important for reducing the limitations regarding Re . Further work will be to investigate if similar trends regarding Re independence for net panels with biofouling is present, and the importance of Sn and

θ .

Secondly, it is emphasized by Lader et al. (2015), Sæther (2015) and this master thesis, that a measurement of the stiffness of a live specimen hydroid stem and multifilament fishing line is necessary. The stiffness is critical for the deflection of the hydroids, and will cause differences in the measured forces. A quantitative comparison of the hydroid stiffness will be very interesting, and give greater assurance in the making of artificial replicas.

Most importantly, it is recommended to use the data presented in the results and perhaps for larger velocities, to estimate an empirical formula dependent on solidity and angle of attack. The trend lines with dependency on solidity and angle of attack, should be optimized to give one curve fit. The curve should be valid for common ranges solidity and angle of attack. If such a formula is achieved, it can be implemented in NS9415.

Bibliography

- Blevins, R. D., 2003. Applied fluid dynamics handbook, reprint ed. with corrections. Edition. Krieger Publ, Malabar, Fla, Ch. Fluid Dynamic Drag, p. 279.
- Blöcher, N., 2013. Biofouling in the norwegian salmon farming industry. Ph.D. thesis, Norwegian University of Science and Technology, Faculty of Natural Sciences and Technology, Department of Biology.
- Carl, C., Guenther, J., Sunde, L., 2011. Larval release and attachment modes of the hydroid ectopleura larynx on aquaculture nets in norway. *Aquaculture Research* 42 (7), 1056–1060.
- De Nys, R., Guenther, J., 2009. The impact and control of biofouling in marine finfish aquaculture-8. In: *Advances in marine antifouling coatings and technologies*. Woodhead Publishing, pp. 177–221.
- Fredheim, A., 2005. Current forces on net structures. Ph.D. thesis, NTNU Department of Marine Technology, Norwegian University of Science and Technology.
- Fredheim, A., Langan, A., 2009. *Advances in technology for off-shore and open ocean finfish aquaculture*, unpublished.
- Gansel, L. C., Plew, D. R., Endresen, P. C., Olsen, A. I., Misimi, E., Guenther, J., Østen Jensen, 2015. Drag of clean and fouled net panels—measurements and parameterization of fouling. *PLoS ONE* 10 (7).
- Gili, J.-M., Hughes, R., 1995. The ecology of marine benthic hydroids. *Oceanogr. Mar. Biol. Ann. Rev.* 33, 351–426.
- Guenther, J., Fitridge, I., Misimi, E., 2011. Potential antifouling strategies for marine finfish aquaculture: the effects of physical and chemical treatments on the settlement and survival of the hydroid ectopleura larynx. *Biofouling* 27 (9), 1033–1042.
- Guenther, J., Misimi, E., Sunde, L., 2010. The development of biofouling, particularly the hydroid ectopleura larynx, on commercial salmon cage nets in mid-norway. *Aquaculture* 300 (1), 120–127.

-
- Hayward, P., Ryland, J., 1990. The marine fauna of the British Isles and north-west Europe. Oxford University Press.
- Hoerner, S., 1965. Fluid Dynamic Drag. Hoerner Fluid Dynamics.
- Klebert, P., Lader, P., Gansel, L., Oppedal, F., 2012. Hydrodynamic interactions on net panel and aquaculture fish cages: A review. *Ocean Engineering* 58, 260–274.
- Lader, P., Dempster, T., Fredheim, A., Jensen, A., 2008. Current induced net deformations in full-scale sea-cages for atlantic salmon (*salmo salar*). *Aquacultural Engineering* 38 (1), 52–65.
- Lader, P., Enerhaug, B., 2005. Experimental investigation of forces and geometry of a net cage in uniform flow. *IEEE Journal of Oceanic Engineering* 30 (1), 79–84.
- Lader, P., Fredriksson, D., Guenther, J., Volent, Z., Blocher, N., Kristiansen, D., Gansel, L., Decew, J., 2015. Drag on hydroid-fouled nets — an experimental approach. *China Ocean Engineering* 29 (3), 369–389.
- Løland, G., 1991. Current forces on and flow through fish farms. Ph.D. thesis, Norwegian University of Technology, Division of Marine Hydrodynamics.
- Moe-Føre, H., Lader, P., Lien, E., Hopperstad, O., 2016. Structural response of high solidity net cage models in uniform flow. *Journal of Fluids and Structures* 65, 180–195.
- Norwegian Directorate of Fisheries, 2017. Key figures from aquaculture industry.
- NTNU, n.d. Marine cybernetics teaching laboratory. <https://www.ntnu.edu/imt/lab/cybernetics>, assessed: 07-02-2019.
- Olafsen, T., 2006. Kostnadsanalyse av ulike begroingshindrende strategier. Tech. rep., SINTEF.
- Oppedal, F., Stien, L., Gansel, L., Pascal, K., Lader, P., Guenther, J., Remen, M., Aas, T., Aure, J., Torgersen, T., 2011. Merdmiljø. Havforskningsrapporten, 28–30.
- Pettersen, B., 2018. Marin teknikk 3 Hydrodynamikk. Akademika, Trondheim, Nor, Ch. 1, 2, pp. 1.22, 2.32.
- Savio, L., 2019. Personal communication in email.
- Steen, S., 2014. Experimental methods in Marine Hydrodynamics. NTNU, Marine technology centre, Trondheim, Nor.
- Sunden, B., 2011. Tubes, crossflow over. <http://www.thermopedia.com/content/1216/>, assessed: 22-02-2019.
- Sæther, A. K., 2015. An experimental investigation on bio-fouling induced drag. Master's thesis, Norwegian University of Science and Technology, Department of Marine Technology, Trondheim.

Appendix

5.3 Flow past a dipole

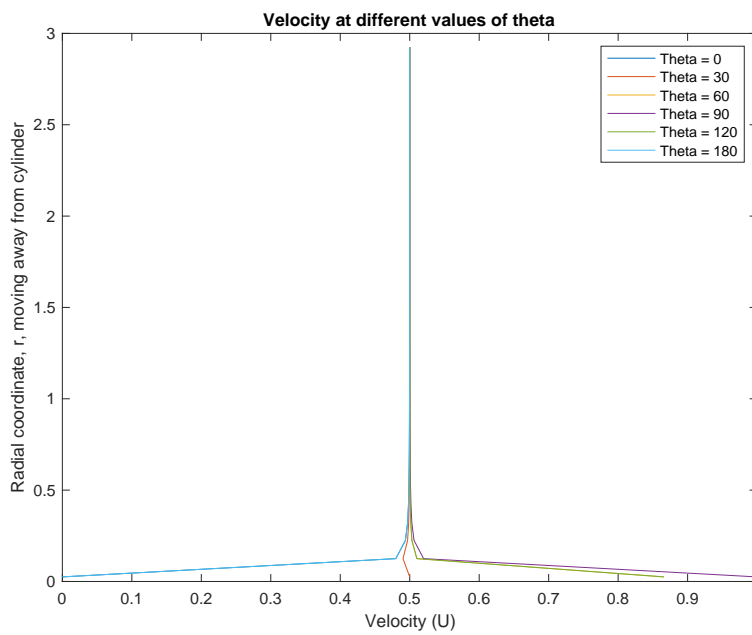


Figure 5.1: Wake past dipole

5.4 Production

Equipment	Name	Details
Glue and sealant	Novatio Seal & Bond MS 60	Used to seal threads to rod. 2mm stripe was used. Had to dry for 10 hours
Handburner for thread	Rosenberger tauwerk gmbh	Used to cut thread which were coiled to a rod.
Electric drill	Panasonic Drill&Driver 15.6V	Used for coiling thread and twisting steel rods.
Small cable ties	Anslut cable tie set	Used to tie steel rods together when the seal was set to dry.
Multifilament fishing thread	250 m Sufix GYRO Deep Green PE 2.5	Used to model hydroids

Table 5.1: Equipment used in the process of making the twines

5.5 List of Excel sheets and Matlab codes

Files in Excel

- estimation.xlsx : calculation of expected forces on the net panels.
- experiment.xlsx : Layout of experiments and time estimation.
- frame.xlsx : Steady state for all measurements for the frame alone. Also includes repeated tests. Each sheet represent an angle of attack.
- net_bio.xlsx : Steady state for all measurements for the fouled net panel and frame. Also includes info about number of twines, length, diameter, area of twine, spacing/half mesh, kinetic viscosity and density of water.
- net_clean.xlsx : Steady state for all measurements for the clean net panel and frame. Also includes info about number of twines, length, diameter, area of twine, spacing/half mesh, kinetic viscosity and density of water.
- vert_bio.xlsx : Steady state for all measurements for the vertical twines with fouling and frame. Also includes info about number of twines, length, diameter, area of twine, spacing/half mesh, kinetic viscosity and density of water.
- vert_clean.xlsx : Steady state for all measurements for the clean vertical twines and frame. Also includes info about number of twines, length, diameter, area of twine, spacing/half mesh, kinetic viscosity and density of water.
- hor_bio.xlsx : Steady state for all measurements for the horizontal twines with fouling and frame. Also includes info about number of twines, length, diameter, area of twine, spacing/half mesh, kinetic viscosity and density of water.
- hor_clean.xlsx : Steady state for all measurements for the clean horizontal twines and frame. Also includes info about number of twines, length, diameter, area of twine, spacing/half mesh, kinetic viscosity and density of water.
- plot.xlsx : Calculates average coefficients independent of Re from data of experimental coefficients from Matlab. Compared trend lines to estimation on clean nets by Løland (1991).

Scripts in Matlab

- catman_read_5r8.m : function to read .BIN file
- frameSpeed.m : reads time interval from excel, cleans data and plots whole time series with steady state. Considers different speeds for a common angle. Calls on *plotTSandForce*, *stats* and *psd*.
- stats.m : function which takes out new vectors from steady state intervals and calculated mean force and velocity, and standard deviation.
- plotTSandForcem.m : function which plots speed, position vs time in subfigure one and force vs time in subfigure two. Saves the time series.

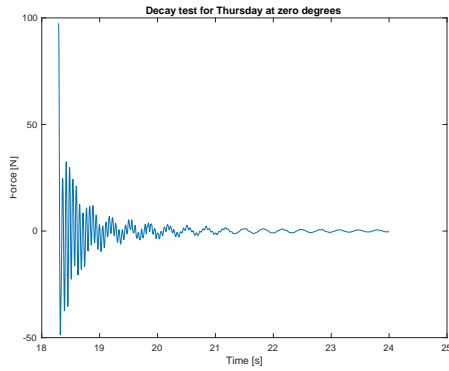
-
- `psd.m` : function plotting power spectral density of the time series and finding maximum peak.
 - `analysis_twineSpeed.m` : Loads results from frame at given speed. For each excel file it imports steady state, cleans data and calculates mean forces. Force contribution on frame is subtracted from total force. The drag per twine and drag coefficient is also calculated. Results are saved and plotted. Calls on *stats*, *plotTSandForcem* and *psd*.
 - `repeat_test.m` : analyzing the uncertainty of the repeated tests. Calls on functions *stats*, *plotTSandForcem* and *psd*.
 - `netforceSpeed.m` : imports saved results from all configurations; net, horizontal and vertical twines. Calculates drag and lift on net section for all velocities and angles of attack. Plots drag and lift on net section against velocity. Clean and fouled net sections are combined in one figure.
 - `Sn_net.m` : imports saved results from all configurations; net, horizontal and vertical twines. Also calculates drag and lift on net section for all velocities and angles. Calculates drag and lift coefficients based on velocity and angle of attack. Then sorts data based on solidity. The drag and lift coefficients based on Løland (1991) formula is calculated, and the drag coefficients from Lader et al. (2015), with 16 mm fouling. Experimental drag- and lift coefficients are plotted vs Reynolds number and compared to both estimates.

Folders in Matlab

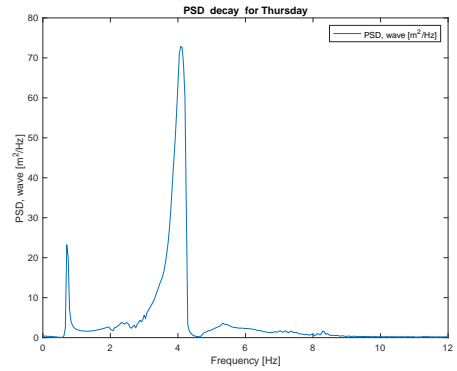
- `data`: stores all binary files from the experiment. They are sorted by bio or clean net, frame, rep and decay.
- `fig`: stores all figures saved in Matlab scrips. Timeseries, includes all time series for every test and a folder for all the PSD associated. Decay, contains only decay time series and PSD. The folder `w_error`, stores any window error computed. Singleruns, consists of figures of the total drag and lift force over speed, for each configuration. The last folder, `multiple`, includes the forces on fouled and clean net and the calculated coefficients.

5.6 Post processing

Decay tests

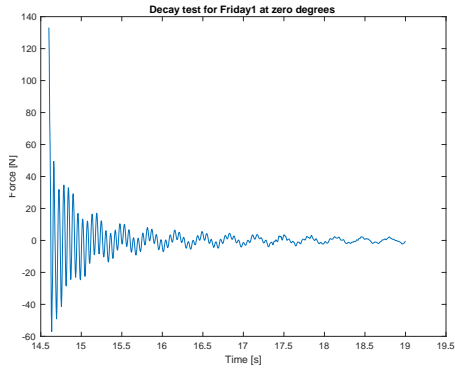


(a) Timeseries

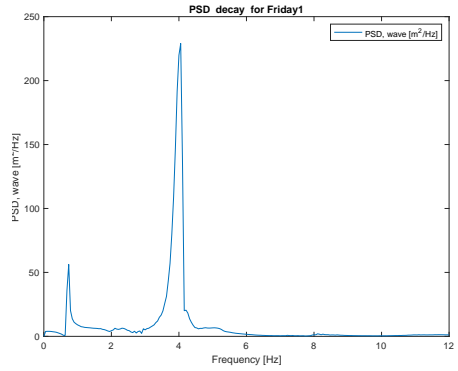


(b) PSD

Figure 5.2: Thursday at 0°

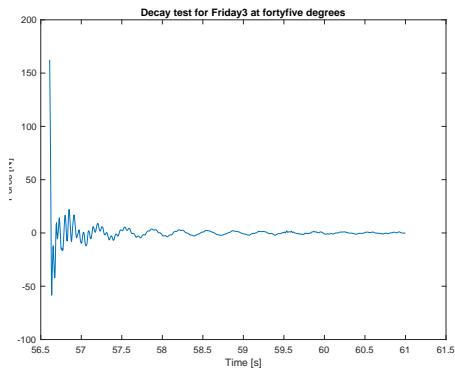


(a) Timeseries

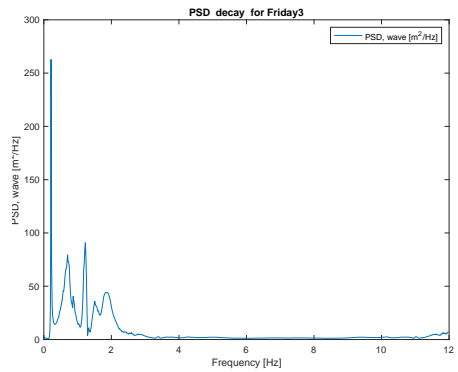


(b) PSD

Figure 5.3: Friday at zero°



(a) Timeseries



(b) PSD

Figure 5.4: Friday at 45°

5.7 Uncertainty

Configuration	Speed [m/s]	Angle [°]	Total velocity [N]			Average \bar{X} [N]
			Run1	Run 2	Run 3	
8bionet	0.35	45	0.3584	0.3584	0.3584	0.3584
6ftb - vert	0.05	45	0.05119	0.05118	0.05118	0.05118
6ftb - vert	0.10	45	0.1024	0.1024	0.1024	0.1024
6ftb - vert	0.20	45	0.2048	0.2048	0.2048	0.2048
7ft - hor	0.25	0	0.2559	0.256	0.256	0.256
7ft - hor	0.30	0	0.3072	0.3072	0.3072	0.3072

Table 5.2: Carriage speed data

5.8 Coefficients on clean twines

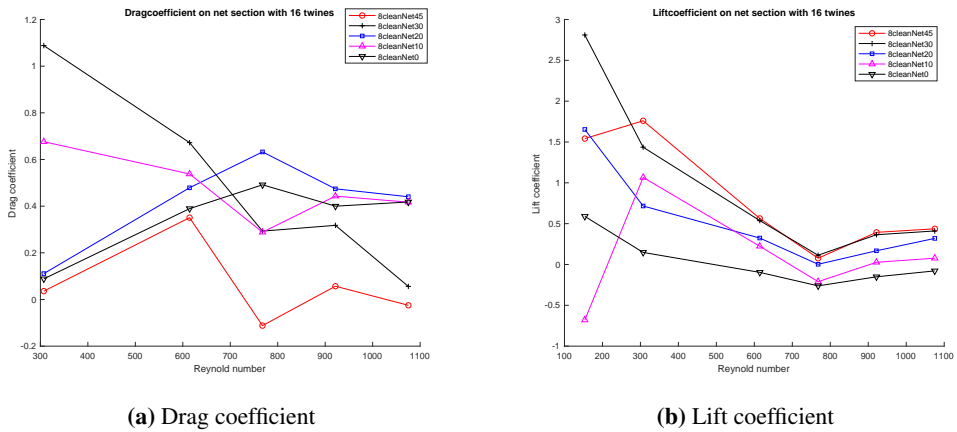
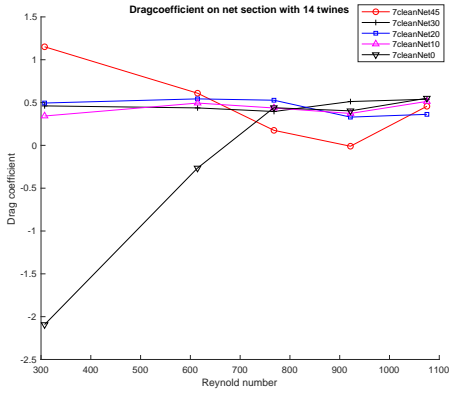
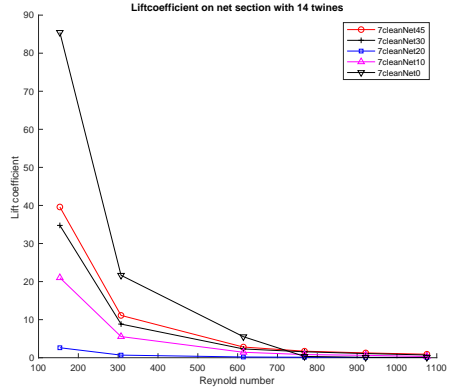


Figure 5.5: 16 twines, $Sn = 0.2820$

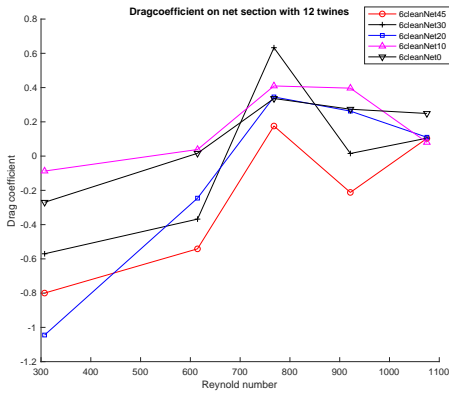


(a) Drag coefficient VS Re for 14 twines

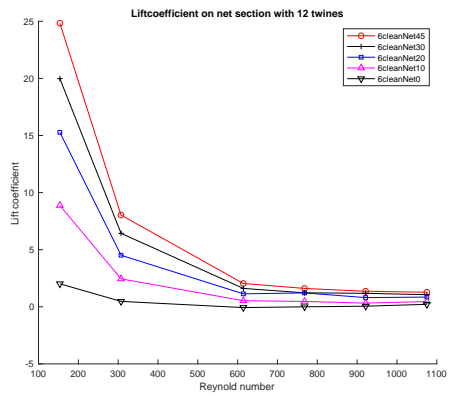


(b) Lift coefficient VS Re for 14 twines

Figure 5.6: 14 twines, $Sn = 0.2359$



(a) Drag coefficient VS Re for 12 twines

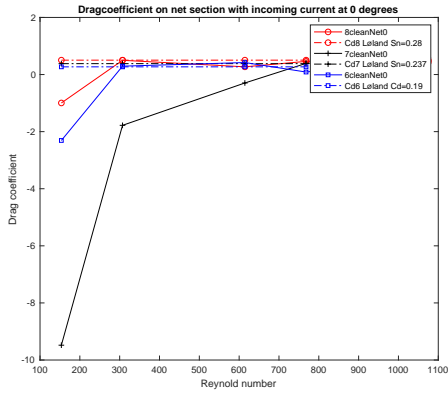


(b) Lift coefficient VS Re for 12 twines

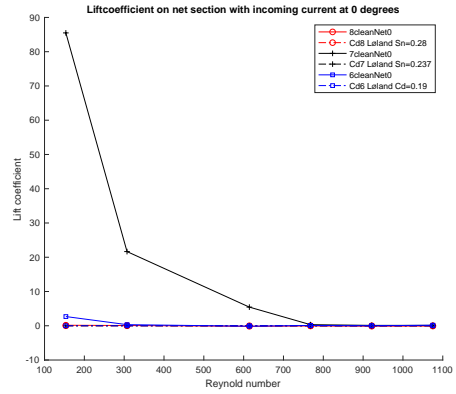
Figure 5.7: 12 twines, $Sn = 0.1989$

5.9 Comparison with Løland

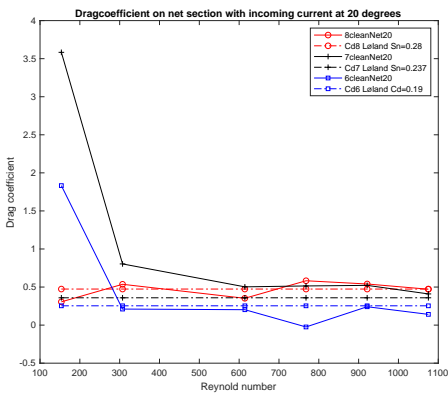
Drag on clean nets



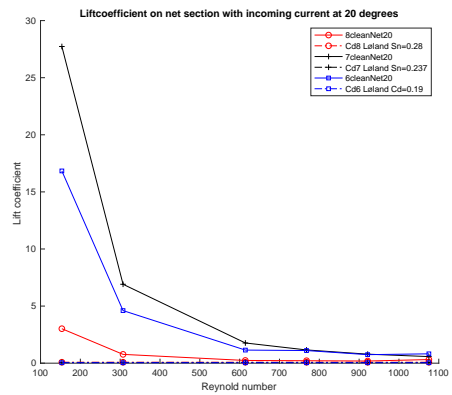
(a) Drag coefficient at 0°



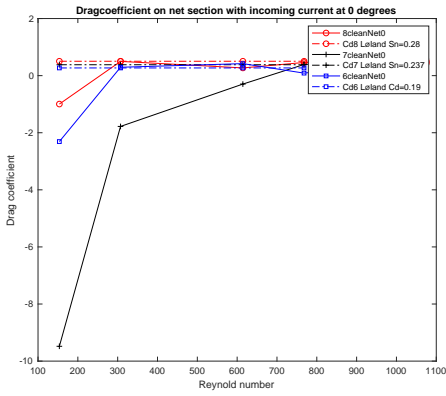
(b) Lift coefficient at 0°



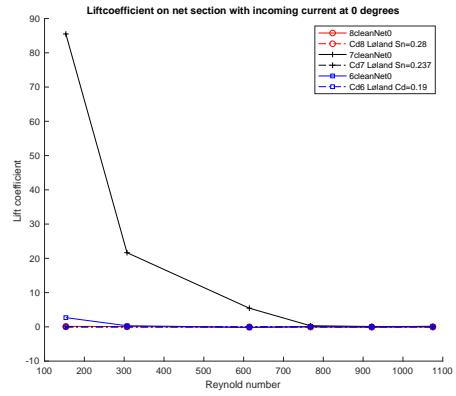
(a) Drag coefficient at 20°



(b) Lift coefficient at 20°

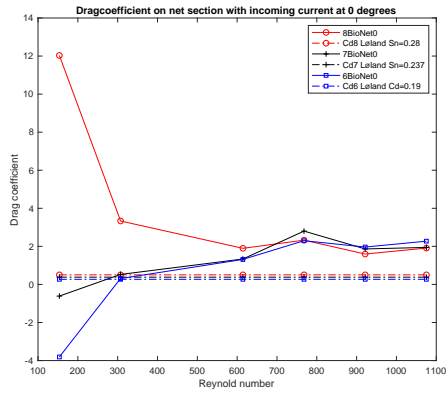


(a) Drag coefficient at 30°

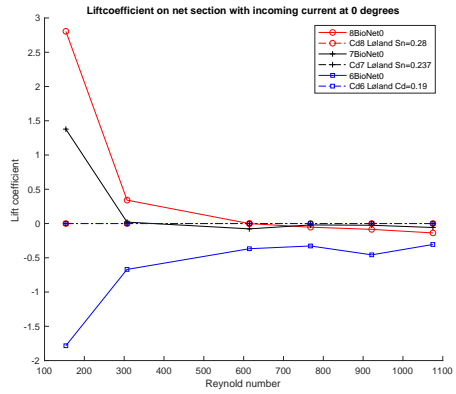


(b) Lift coefficient at 30°

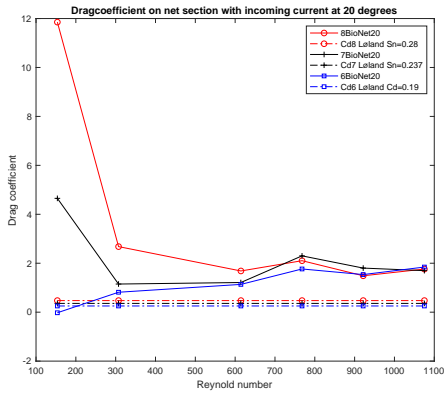
Twines with biofouling



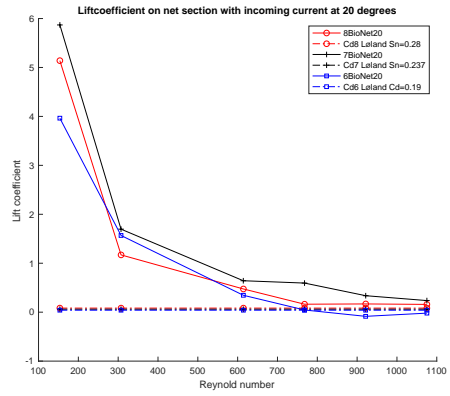
(a) Drag coefficient at 0°



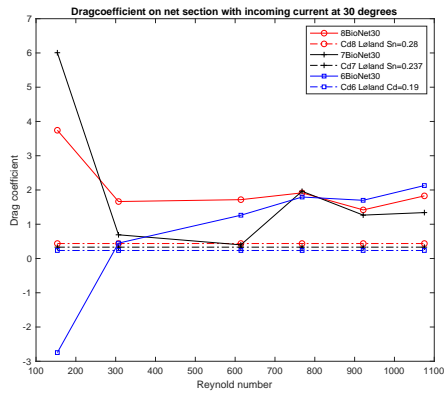
(b) Lift coefficient at 0°



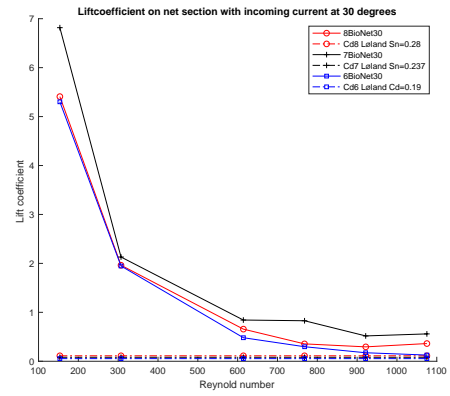
(a) Drag coefficient at 20°



(b) Lift coefficient at 20°



(a) Drag coefficient at 30°



(b) Lift coefficient at 30°

5.10 Functions of trend lines

Drag on clean and 16 mm hydroid fouled twines

X- is the angle of attack, calculated in degrees. Y- is the solidity. Coefficient on clean net is given first, then the fouled net.

For solidity of 0.19

$$C_D = -0,00007 * x^2 + 0,0029 * x + 0,1602 \quad (5.1)$$

$$C_D = -0,0004 * x^2 - 0,0018 * x + 1,6718 \quad (5.2)$$

For solidity of 0.237

$$C_D = -6E - 05 * x^2 - 0,0003 * x + 0,453 \quad (5.3)$$

$$C_D = -0,0006 * x^2 + 0,0097 * x + 1,7362 \quad (5.4)$$

For solidity of 0.28

$$C_D = -0,0001 * x^2 + 0,0047 * x + 0,43 \quad (5.5)$$

$$C_D = -0,0002 * x^2 - 0,0108 * x + 2,2159 \quad (5.6)$$

For angle of attack = 0°

$$C_D = 2,9162 * y - 0,3299 \quad (5.7)$$

$$C_D = 6,3835 * y + 0,3418 \quad (5.8)$$

For angle of attack = 20°

$$C_D = 2,8008 * y - 0,3073 \quad (5.9)$$

$$C_D = 5,8043 * y + 0,2971 \quad (5.10)$$

For angle of attack = 30°

$$C_D = 3,3434 * y - 0,4071 \quad (5.11)$$

$$C_D = 2,5316 * y + 0,8393 \quad (5.12)$$

For angle of attack = 45°

$$C_D = 2,369 * y - 0,2896 \quad (5.13)$$

$$C_D = 5,4248 * y - 0,1797 \quad (5.14)$$

Drag coefficients from Løland (1991)

X- is the angle of attack, calculated in degrees. Y- is the solidity.

For solidity of 0.19

$$C_D = -3E - 05 * x^2 - 6E - 05 * x + 0,2654 \quad (5.15)$$

For solidity of 0.237

$$C_D = -5E - 05x^2 - 1E - 04 * x + 0,3808 \quad (5.16)$$

For solidity of 0.28

$$C_D = -6E - 05x^2 - 0,0001 * x + 0,4983 \quad (5.17)$$

For angle of attack = 0°

$$C_D = 2,5834 * y - 0,2275 \quad (5.18)$$

For angle of attack = 20°

$$C_D = 2,4276 * y - 0,2114 \quad (5.19)$$

For angle of attack = 30°

$$C_D = 2,2373 * y - 0,1917 \quad (5.20)$$

For angle of attack = 45°

$$C_D = 1,8267 * y - 0,1492 \quad (5.21)$$

